COMBINING VIBRATIONAL LINEAR-BY-PART DYNAMICS AND KINETIC-BASED DECOUPLING OF THE DYNAMICS FOR MULTIPLE ELASTOPLASTIC SMOOTH IMPACTS

Ana Barjau, Joaquim A. Batlle and Josep M. Font-Llagunes

Department of Mechanical Engineering and Biomedical Engineering Research Centre
Universitat Politècnica de Catalunya, Diagonal 647, 08028 Barcelona
Phone: +34 934 016 716, Fax: +34 934 015 813
e-mail: ana.barjau@upc.edu, agullo.batlle@upc.edu,
josep.m.font@upc.edu

Keywords: multiple-point impact; contact dynamics; modal analysis; constraints; elastoplasticity

Abstract. *This article proposes a linear-by-part approach for elastoplastic 3D multiple-point smooth impacts in multibody systems with perfect constraints. The model is an extension of a previous version, restricted to the perfectly elastic case, able to account for the high sensitivity to initial conditions and for redundancy without assuming any particular collision sequence [1]. Energy losses associated with compression and expansion in percussive analysis is a matter as complex as the physical phenomena involved, at the nanoscale level, for different materials. Simplified models can be developed for specific purposes, which can retain the most relevant trends of internal damping and at the same time be suitable for a particular analytical approach of impact mechanics. In the context of this article, energy dissipation due to material deformation is introduced through a linear-by-part elastoplastic model consisting on two elementary sets of springs and dry-friction dampers. The first set accounts for inelastic behavior (energy loss without permanent indentation), while the second one introduces plasticity (that is, permanent indentation). In inelastic and plastic collisions, instantaneous unilateral constraints may appear, thus reducing the number of degrees of freedom (DOF) of the system. The calculation of the corresponding normal contact force at the constrained points is then necessary in order to detect whether the constraint holds or disappears (either because a new compression or an expansion phase starts, or because contact is lost). Different simulated application examples are presented and thoroughly discussed.*

1 INTRODUCTION

Impact problems are often encountered in different branches of mechanics. They appear in robotics (robot-robot or robot-environment interaction), in physics of granular media, in biomechanics (heel-ground collisions in human gait analysis), or in musical acoustics (hammer-string collisions, stick-drum collisions), among others.

Essentially, an impact consists of a sudden change of mechanical state usually implying some degree of energy loss. Though sharing this essential feature, different approaches have been proposed to study and simulate impacts [2, 3].

Impacts may generate waves propagating from the colliding point and reaching all other points in the system. When the impact duration is larger than the period of the lowest vibration mode of the colliding bodies, that phenomenon can be neglected and the system can be treated as a rigid-body system. When this is not the case, the system flexibility has to be taken into account and the impact problem is usually studied through a finite-element method. The propagating waves are responsible for trapping a fraction of the initial energy. [4]

For the case of rigid-body systems, the unavoidable deformation associated with impact is localized at the colliding points, and the overall configuration may be assumed to be constant throughout the collision interval. Consequently, rigid-body models are in principle less demanding than flexible-body ones from the computational point of view.

The approaches found in literature to study collisions in rigid-body systems can be roughly classified into variable-configuration (VC) approaches and constant-configuration (CC) ones. VC methods rely on compliant models to explore the interactions at the colliding points. The equations of motion are integrated during the impact interval (typically through a Finite Elements method), and neither the impact duration nor the system's final mechanical state is known beforehand.

In CC methods, as the time interval elapsed between the beginning and the end of the impact is very small (as compared to the time scale of non-impact dynamics), the system configuration is assumed to be constant. For the case of single-point smooth collisions, the use of coefficients of restitution (COR) leads to the post-impact velocities without need of any compliant model, and the problem is formulated through purely algebraic equations.

Single-point rough collisions cannot be treated in the same way. If tangential compliance is not considered, these problems are usually treated through Routh and Darboux methods. The more relevant feature of these methods is the use of the normal impulse as the integration variable (instead of time) to determine the velocity changes. This allows the determination of the velocity changes without using any particular compliant model but does not give any information about the value of the force at the collision point. Consequently, the detection of the collision end (which corresponds to a zero force value) has to be established through a plausible hypothesis concerning energy losses, usually formulated through a COR.

Those methods have to be used with caution in single-point rough impacts. On one hand, the use of Newton's and Poisson's COR may be energetically inconsistent [5], and the energetical COR needs to be generalised for the dual compression case [6]; on the other hand, for the case of rough collisions, the impulse associated with the friction force is not proportional to that associated with the normal force whenever the sliding direction changes within the impact interval [7].

The aforementioned methods may not be applicable to multiple-point collisions [8]. In that case, the use of a compliant model is unavoidable. The constitutive laws allow the time integration of the equations of motion (simplified by the CC hypothesis) thus yielding the evolution of both velocities and normal forces at the collision points. The advantage of that integration is the easy detection of the collisions end, which is certainly one of the important aspects that have to be dealt with cautiously in impact dynamics (as stated in [9]).

In general, the correct detection of the collision end at a particular point has to be done through the analysis of the associated force and separation velocity at that point. Only when that force takes a zero value and that velocity is positive can we say that the collision at that point is over.

That condition depends not only on the local contact characteristics and the global inertia properties of the colliding bodies but also on the wave effects [9]. In the present work, we develop a model which does not consider the possibility of wave generation as we treat the colliding bodies as globally rigid.

As mentioned before, a rather common formulation of the end detection is that of the energetic COR. However, in multiple point collisions it may lose its meaning because some

points may undergo several compressions before the impact is totally over. In that case, the energy dissipation ratio may depend on the compression-expansion phases evolution, and thus the hypothesis of an energetic COR associated to each contact point is not valid.

Some authors [8, 9], though, follow Routh and Darboux approaches for multiple point-collisions and use the normal impulse at one selected collision point as integration variable. To do so, they define an impulse correlation rule based on the constitutive law. The choice of a particular collision point may lead to numerical problems (for instance, if the impulse at that point becomes much smaller than the impulses at the other collision points) which can be overcome by increasing the time-integration complexity [10]. On the other hand, the collision end is not detected through that integration, and one COR per contact is used.

Two important features appear when dealing with multiple-point collisions, which are not possible in single-point ones:

- in both smooth and rough collisions, redundancy may appear if the normal velocities of some colliding points are linearly related [12, 13].

- in elastoplastic and inelastic impacts (that is, with and without permanent indentation, respectively), permanent or instantaneous unilateral constraints may appear, thus reducing the system's number of degrees of freedom.

The aim of the present study is to propose an efficient method to simulate smooth 3D multiple-point collisions in multibody systems with perfect constraints able to overcome those difficulties. In a previous work, we developed a version of this approach, restricted to elastic impacts, able to cope with redundancy [1]. The main idea consisted of assuming a finite linear normal stiffness (high enough to assume constant configuration throughout the process) at each impact point and solving a vibrational problem. Two different time and space scales were used. At the macro scale, the overall system configuration was assumed to be constant. Consequently, the inertia and Jacobian matrices appearing in the formulation were also constant. That previous approach can cope with redundancy, that is, can be used to treat situations where the normal velocities of some colliding points are linearly related. In this work, we present an extension that includes energy dissipation (with or without permanent indentation).

Energy loss mechanisms may vary from one problem to another as they depend strongly on the mechanical characteristics of the colliding materials. In systems without tangential friction, the energy dissipation is mainly associated with material damping and material plasticity (leading to permanent indentation). At high impact velocities, the effect of plasticity predominates over the material damping mechanism [14, 15] (though plasticity effects may also occur at relatively moderate pre-impact velocities).

Mechanical models of interconnected springs and dampers have been widely used to account for the material viscoelastoplastic characteristics. Biot justified the interest of such models in general from thermodynamic considerations [16].

The simplest model is probably Kelvin-Voigt's model, consisting of a parallel association of a linear spring and a linear damper. The main interest of that model is its all-linear behaviour, thus allowing straightforward analytical solutions. That model, when applied to impacts, has three main drawbacks: the normal force discontinuity at the beginning of the collision (associated with its velocity dependence), the impossibility of reproducing collisions with permanent indentation and the possibility of involving negative contact forces.

Variations of Kelvin-Voigt's model consist on replacing the linear spring and damper by nonlinear ones (for instance, a Hertz's compliant formulation for the spring [17], or an indentation-dependent viscous damper [18, 19, 20]), but this does not allow the simulation of permanent indentation.

Energy loss can also be introduced through a partially-latching spring [21, 22, 23, 24]. During loading (compression phase), the stiffness is higher than during unloading (expansion phase). Inelasticity is inherent to the model, but dissipative collisions without permanent indentation are not covered.

More elaborate models may account both for dissipative collisions with or without permanent indentation. The transition from one case to the other implies the consideration of a yield point (see, for example, [25, 26, 27, 28, 29])

Finally, hysteretic memory-dependent models have also been proposed. Maybe the most well-known is the Bouc-Wen model, a good survey of which can be found in [30].

Our goal was to cover the whole range of dissipative collisions (with or without permanent indentation) through a simple formulation (not relying on nonlinear elementary elements). The result has been a piecewise linear elastoplastic compliant model compatible with the vibrational algorithm presented in [1]. The model is able to cope with redundancy and with a variable number of system's DOF associated to the creation and/or disappearance of unilateral constraints.

The compliant model at each collision point consists of two elementary sets of spring and dry-friction damper, with friction force modulus proportional to the spring force, responsible for a hysteretic material behaviour. One set accounts for inelastic behaviour, while the other one introduces plasticity. A suitable choice of parameters allows the model to cover from perfectly elastic to perfectly plastic (that is, with no expansion phase at all) impacts. As the springs are linear and the dampers dry-friction force is proportional to the spring force, both the compression and the expansion are strictly linear, whereas the whole cycle is globally nonlinear.

Our model has been validated through the tuning of the model parameters in order to fit our simulations to results found in the literature (coming either from more elaborated models or from experimental measurements).

The article is organized as follows:

- Section 2 presents a brief summary of the linear-by part approach presented in [1].
- Section 3 develops the details of the compliant model.
- Section 4 is devoted to the tuning of the model parameters through comparison with other authors' results.
- Section 5 explains how to deal with the creation/disappearance of unilateral constraints and the subsequent eventual reduction of DOF.
- Section 6 presents different application examples.
- Section 7 contains the final discussion and conclusions of the work.

The formulation we present applies to both 2D and 3D problems. However, we have chosen just planar examples because the results are more easily understood. Explaining and following the different expansion/compression phases in a 3D problem is far less simple and thus less appropriate to highlight the interesting features of our approach.

2 THE LINEAR-BY-PART APPROACH

Let's consider an *n*-DOF multibody system, described by the *n* vector of generalized velocities $\mathbf{u}$, undergoing a simultaneous collision at *m* contact points Q_i. The *m* normal separation velocities at those contact points $\dot{\boldsymbol{\delta}}$ (being $m \le n$ or $m \ge n$) are related to the generalized velocities $\mathbf{u}$ through a $m \times n$ Jacobian matrix of kinematic coefficients, $\dot{\boldsymbol{\delta}} = \mathbf{A}(\mathbf{q})\mathbf{u}$ (of course, matrix $\mathbf{A}$ depends on the coordinates in general: $\mathbf{A}(\mathbf{q})$; however, as configuration is assumed to be constant throughout the impact, we will write it just as $\mathbf{A}$ for the sake of simplicity). We will consider first that the *m* normal velocities are independent (that is, the system presents no redundancy) and, consequently, $\text{rank}(\mathbf{A}) = m \le n$.

The reduced formulation of the vibration problem associated with the normal displacements is given by:

$$\mathbf{M}_n \ddot{\boldsymbol{\delta}} + \mathbf{K}_n \boldsymbol{\delta} = 0 \tag{2.1}$$

where $\mathbf{M}_n \equiv \left(\mathbf{A}\mathbf{M}_u^{-1}\mathbf{A}^T\right)^{-1}$, being $\mathbf{M}_u$ the $n \times n$ inertia matrix for the impact configuration, $\mathbf{K}_n$ is a diagonal stiffness matrix with elements $k_j > 0$ if there is indentation at the contact point Q_j, and $k_j = 0$ otherwise. The parameter k_j and the variable δ_j are the stiffness and the normal displacement at the contact point (thus, indentation is associated with negative displacement).

The eigenvalues and eigenvectors of the dynamical matrix $\mathbf{D} \equiv \mathbf{M}_n^{-1}\mathbf{K}_n$ define the eigenfrequencies and eigenmodes of the vibration problem.

If the m normal separation velocities at the contact points Q, $\dot{\boldsymbol{\delta}}$, are not independent, $\mathrm{rank}(\mathbf{A}) < m$ (regardless of being $m \le n$ or $m \ge n$). We say then that the system presents *redundancy*.

Among the m contact points, it is always possible to choose a subset whose normal velocities are independent. Let's take $\{\dot{\delta}_1 \quad ... \quad \dot{\delta}_p\}^T = \mathbf{A}_{ind}\mathbf{u}$ (with $p \le n$) to be the independent normal velocities at the colliding points. The normal velocities of the other contact points can be related to the previous subset through a matrix **R** (or *redundancy* matrix):

$$\{\dot{\delta}_{m-p} \quad ... \quad \dot{\delta}_m\}^T = \mathbf{R}\{\dot{\delta}_1 \quad ... \quad \dot{\delta}_p\}^T \Rightarrow \dot{\boldsymbol{\delta}}_{rel} = \mathbf{R}\dot{\boldsymbol{\delta}}_{ind} \ . \tag{2.2}$$

The reduced formulation of the vibration problem associated with the normal displacements is now given by

$$\tilde{\mathbf{M}}_n\ddot{\boldsymbol{\delta}}_{ind} + \tilde{\mathbf{K}}_n\boldsymbol{\delta}_{ind} = 0 \ , \tag{2.3}$$

where $\tilde{\mathbf{M}}_n \equiv \left(\mathbf{A}_{ind}\mathbf{M}_u^{-1}\mathbf{A}_{ind}^T\right)^{-1}$, being $\mathbf{M}_u$ the $n \times n$ inertia matrix for the impact configuration, and

$$\tilde{\mathbf{K}}_n = \begin{bmatrix} k_1 & & \\ & ... & \\ & & k_p \end{bmatrix} + \mathbf{R}^T \begin{bmatrix} k_{m-p} & & \\ & ... & \\ & & k_m \end{bmatrix} \mathbf{R} \ . \tag{2.4}$$

If the indentation at the contact point Q_j is nonzero ($\delta_j < 0$), then $k_j > 0$. If there is no indentation ($\delta_j \ge 0$), then $k_j = 0$.

Again, the eigenvalues and eigenvectors of the dynamical matrix $\tilde{\mathbf{D}} \equiv \tilde{\mathbf{M}}_n^{-1}\tilde{\mathbf{K}}_n$ define the eigenfrequencies and eigenmodes of the vibration problem.

3 THE ELASTOPLASTIC MODEL

In order to keep the linear-by-part essence of the lossless approach presented in [1], the dissipative characteristics of the colliding surfaces have been modeled through a combination of linear springs and dry-friction dampers. As mentioned in the previous section, viscous damping yields energy losses but does not allow permanent indentation at the collision points.

Dry-friction dampers can account for plasticity. The elementary system consisting of a linear spring (with stiffness k) and a dry-friction damper shown in Fig.1(a) is the basis of our model. The friction force value is taken to be proportional to that of the spring through a friction coefficient μ: $|F_{fric}| = \mu F_{spring} = \mu k x$ Note that the force is independent of $|\dot{x}|$ because it is a dry friction model, not a viscous one. Fig.1(b) shows the total force generated by that system as a function of the deformation x (or indentation) for the case $0 < \mu < 1$ (note that coordinate x and coordinate δ have opposite signs). During compression, the total force is given by the addition of that of the spring and that of the dry-friction damper:

$$N^{comp} = kx + \mu kx \equiv k^{comp} x \quad . \tag{3.1}$$

During expansion, those two forces have opposite signs, and so the expansion force takes a lower value:

$$N^{exp} = kx - \mu kx \equiv k^{exp} x \quad . \tag{3.2}$$

The transition from compression to expansion implies then a sudden decrease of the total force with value $|\Delta N| = 2\mu kx$. The dissipated energy coincides with the grey-shaded area.

The evolution of the deformation at the collision point (P) is governed by the dynamics of the rigid body to which point P belongs. For the case of multiple-point collisions, then, that dynamical behaviour can be rather complex, and any point reaching the $\dot{x} = 0$ condition may either undergo further compression, start an immediate expansion or be constrained during a certain time by the effect of other impact forces (applied to other impact points). The investigation of those potential three different behaviours calls for the calculation of the normal contact force needed to keep the $\dot{x} = 0$ condition at that point at that particular configuration. The

details of such a calculation are presented in section 5, but a few qualitative examples will be presented now.

For clarity sake, we will consider first the two cases $\mu = 0$ and $\mu \geq 1$, and then comment the intermediate case $0 < \mu < 1$. Fig.2 shows the qualitative different behaviour associated with the $\mu = 0$ and $\mu \geq 1$ cases:

- $\mu = 0$ corresponds to a perfectly elastic material (Fig.2(a)). Compression and expansion phases take place according to a same slope $\left(k^{comp} = k^{exp} = k\right)$. Once a first compression is initiated, a zero velocity $\left(\dot{x} = 0\right)$ will indicate the beginning of an expansion. The latter may be total (that is, leading to a zero deformation $x = 0$) or partial, as it may be stopped by collisions at other points of the same rigid body. In that case, the deformation at P would evolve along the line in Fig.2(a) until eventually a total expansion would be completed and the non-deformed configuration $x = 0$ would be reached. No permanent deformation is possible.

- $\mu \geq 1$ corresponds to a perfectly plastic material (Fig.2(b)), that is: expansion is not possible. In this case, the compression stiffness is calculated as before, $k^{comp} = (1+\mu)k \geq 2k$, whereas the expansion one is directly set to zero, $k^{exp} = 0$ (it cannot be calculated through equation (3.2), as it would yield a negative value thus introducing energy into the system instead of dissipating it). The indentation x_{max} attained at the end of the compression phase is a provisory permanent indentation. The body dynamics may be responsible again for an up-and-down evolution on the vertical line in Fig.2(b). In that case, point P is constrained (zero velocity), and the force value corresponds to that of the constraint force needed to maintain that constraint.

Fig. 3 describes the possibility of a constraint for the case $0 < \mu < 1$. In Fig.3(a), point P completes the cycle returning to the zero indentation situation but having spent some time in a constrained situation (up and down the vertical line with $\dot{x} = 0$) . However, for the case shown in Fig.3(b), the first expansion (black) is not completed as a new compression phase

starts when the indentation has not yet reached the zero value. That second compression phase (red) goes on until the condition $\dot{x} = 0$ is reached again (which happens for a higher value of the indentation), and then a second expansion phase starts. According to the body dynamics, that expansion may go on until $x = 0$ (total expansion) or be followed by a third compression (in that case, the second expansion is a partial one).

Note that the elementary system in Fig.1(a) allows the possibility of a permanent deformation only in totally plastic behaviour. In order to allow permanent deformation in non-plastic situations, we propose a model consisting of two series elementary systems (Fig.4), the upper one with stiffness k and friction coefficient $0 \le \mu < 1$ (inelastic system), and the lower one with stiffness k' and $\mu' = 1$ (plastic system).

As shown in Figure 4, the deformation of each elementary system is defined through an absolute coordinate (x for the upper system and x_0 for the lower one). When introducing g a deformation x in the upper system, if the initial value of the lower system coordinate x_0 is zero, both systems undergo a compression (and thus $x_0 \neq 0$) . If having attained a certain value $x_0 \neq 0$ the upper system begins an expansion phase, the lower one will be retained by the dry-friction damper. That lower dry-friction damper, combined with the parallel stiffness k', will be able to generate a maximum force of $2k'x_0$. Only if a new compression of the upper set generates a force higher than $2k'x_0$, will the lower set compress further.

This series arrangement of elementary systems may account for an initial pre-compression (prior to collision). Fig.5(a) shows the generation of that pre-compression. From A to A', both systems deform, and the total effective stiffness is:

$$k^{*comp} = \left(\frac{1}{(1+\mu)k} + \frac{1}{2k'} \right)^{-1} = \frac{k(1+\mu)2k'}{k(1+\mu)+2k'} \quad , \tag{3.3}$$

The velocity at A' is zero, and the total normal force is $N_0 = k^{*comp} x(A') = 2k'x_{01}$. In the subsequent expansion phase, the normal force shows a sudden decrease due to the transition from $k^{*comp} = 2k'$ (point A') to $k^{exp} = k(1-\mu)$ (point A"), and then the plastic system retains its deformation while the deformation of the inelastic one decreases until a zero velocity is at-

tained again at point B. During this phase, the effective stiffness is only related to the inelastic system: $k^{exp} = k(1-\mu)$.

Fig.5(b) shows a possible scenario starting with the pre-compression described in Fig.5(a) (initial normal deformation $x = x_{01}$, initial lower spring force $N_{01} = 2k'x_{01}$). The collision starts with an inelastic phase where just the upper elementary system is responsible for the total normal force at the colliding point: $N_{01} = k^{comp}(x - x_{01}) = (1+\mu)k(x - x_{01})$. If the end of the compression phase ($\dot{x} = 0$) is attained when $N \le N_{01}$, the collision is inelastic and no further permanent deformation appears. This would be the case of the BB'B"B cycle.

However, if $\dot{x} = 0$ for $N > N_{01}$ (that is, if the $\dot{x} = 0$ is attained for $x > x(A')$), the plastic system undergoes a compression and the provisory permanent indentation will increase. The total effective stiffness is now k^{*comp} $(< k^{comp})$, as both systems are undergoing deformation. In the study case presented on Fig.5(b), the compression ends at point D', and transition to expansion implies again a sudden change in the normal force $|\Delta N| = 2\mu k x(D')$. The cycle may end at C, with a permanent indentation $x_{02} > x(C)$ or, having reached C, restart a new compression of just the inelastic system (this is the case of cycle CC'C"C) or go on to values of indentation $x > x(D')$ leading to a new increase of the permanent deformation.

4 TUNING OF MODEL PARAMETERS

Model tuning has been done through comparison with other author's results. Flores *et al.* [20] presented a continuous nonlinear contact force model (based on a Hertz's type spring and a nonlinear viscous damper) suitable both for soft and hard contacts but without permanent indentation. They applied their model to the case of a ball colliding with the ground, and proceeded to simulate a wide range of problems with different values of Newton's coefficient of restitution e.

We have applied our model to the same problem. The colliding ball has the same initial velocity (4 m/s) and the same geometric and inertia parameters than that in [20]: radius 0.1 m,

mass 1 kg and central inertia moment $0.1\,\mathrm{kg}\cdot\mathrm{m}^2$. In order to reproduce impacts without permanent indentation, we have taken a very high value for the stiffness of the plastic spring-damper set (thus its deformation is negligible as compared to that of the other set). The parameter values of the elastic set have been tuned to match the results in [20][1]: a constant stiffness $k = 1000\ \mathrm{kN/m}$ and different values for $\mu(=0,\ 0.22,\ 0.47,\ 0.73,\ 0.93)$ yielding different values for the restitution coefficient $e(=1,\ 0.8,\ 0.6,\ 0.4,\ 0.2)$.

Figures 6(a) and 6(b) show the evolution along the impact interval of the indentation and the approaching velocity respectively. As the collision time microscale is irrelevant, we have normalized the impact interval duration to that of the most dissipative case $(e = 0.2)$. There is a good qualitative coincidence with the corresponding curves in [20], and the quantitative discrepancies are below 11%. Figure 6(c) shows sharps corners associated to the force discontinuity when shifting from compression to expansion. The corresponding curves in [20] do not show that discontinuity, but rounded corners. Nevertheless, the area inside those curves, which represents the dissipated energy, are really close in value.

In order to assess the plastic behavior of our model, we have reproduced the application example presented by Yigit *et al.* in [31]. It consists on a hemispherical steel impactor with a mass of 0.5 kg and a radius of 10 mm colliding against a composite target. We have simulated the same problem with the same values as far as geometry and inertia properties are concerned, but with different values for the elastoplastic parameters. Figures 7(a) and 7(b) show the resulting force-displacement curves for two different impact velocities (0.1 m/s and 1 m/s respectively). In both cases, the resulting permanent deformation and the dissipated energy (area enclosed by those curves) are close to those in [31][2]. Again, the plots obtained by means of our approach show sharp corners which do not appear in Yigit's results. In the present case, they are associated with discontinuities in the contact forces derivatives.

A last comparison has been done between our model and that presented by Seifried *et al.* in [14]. The aim is to verify the qualitative increase of the contact force in a succession of impacts until saturation is reached[3]. Seifried *et al.* use an elastoplastic model and solve the prob-

[1] Figure 6, plots (a), (b) and (d)
[2] Figures 3 and 5 in [31], respectively.
[3] Upper left plot of Figure 5 in [14].

lem of a sphere-to-rod impact through a FE analysis. They also account for vibrations in the colliding bodies.

Our application example consists again of a ball-ground impact. The ball mass and radius are 1 kg and 1 m, and the model parameters take the values $k = k' = 3.5 \cdot 10^3$ kN/m , μ=0 . The impact velocity is always 0.3 m/s. However, impacts differ from one another because of the permanent indentation and subsequent residual stress. Figure 8 shows the evolution along the impact interval of the contact force. For the same reason mentioned before, the impact interval duration has been normalized to that of the first collision.

As in [14], the lowest force peak value and the longest impact interval correspond to the first impact. The second impact duration is about 12% shorter, and the force peak value is some 12% higher. From the fourth collision on, impact duration and force peak value remain roughly the same.

5 INVESTIGATION OF EVENTUAL UNILATERAL CONSTRAINTS

Multiple-point collisions (elastic, inelastic or plastic) in a multibody system are bound to generate transient and/or permanent constraints leading to a transient and/or permanent reduction of its DOF. As mentioned in Section 3, a colliding point reaching a zero-velocity condition may either undergo further compression, start an immediate expansion or be constrained during a certain time by the effect of other impact forces (applied to other impact points). The latter corresponds to the creation of a constraint

The investigation of potential constraints is formulated differently if we are dealing with a nonredundant collision (the normal velocities of the colliding points are independent) or a redundant one (where some of those velocities are linearly related). We will consider first the nonredundant case, as it is simpler, and then generalize for the redundant one. In what follows, we will be talking about normal displacements δ instead of normal deformations x, in order to maintain the same notation as in Section 2, where the previous linear-by-part approach has been summarized. Though $|\delta| = |x|$, during collision the normal displacement is negative ($\delta < 0$) whereas the deformation is positive ($x > 0$).

5.1 Exploration of transient constraints in a nonredundant multiple-point collision

Let's consider, with no loss of generality, that point Q_1 reaches the end of a compression phase ($\dot{\delta}_1 = 0$). If its normal displacement $\delta_1 (< 0)$ lies within the interval $0 \le |\delta_1| \le |\delta_{01}|$ (where $|\delta_{01}|$ is the permanent indentation for that point), the corresponding normal force is $N_1^{comp} = k_1^{comp} |\delta_1| = -k_1^{comp} \delta_1$. If $|\delta_1| > |\delta_{01}|$, $N_1^{comp} = -k_1^{*comp} \delta_1$.

Whether point Q_1 maintains its zero normal velocity (meaning that motion is constrained or, what is equivalent, that a unilateral constraint is created) depends on the system dynamics at that same time instant. Keeping $\dot{\delta}_1 = 0$ calls for a normal force N_1 whose value would be between the compression force N_1^{comp} and the expansion force $N_1^{exp} = -k_1^{exp} (\delta_1 - \delta_{01}) = N_1^{comp} (1 - 2\mu)$. If this is the case, Q_1 behaves as an unilateral constraint, and $\ddot{\delta}_1 = 0$.

The calculation of that contact force is straightforward. If Q_1 is constrained, the system's dynamical equations (Eq. 2.1) become

$$\begin{bmatrix} m_{11} & m_{12} & \dots & m_{1m} \\ m_{21} & m_{22} & \dots & m_{2m} \\ \dots & \dots & \dots & \dots \\ m_{m1} & m_{m2} & \dots & m_{mm} \end{bmatrix} \begin{Bmatrix} 0 \\ \ddot{\delta}_2 \\ \dots \\ \ddot{\delta}_m \end{Bmatrix} = - \begin{bmatrix} 0 & & & \\ & k_2 & & \\ & & \dots & \\ & & & k_m \end{bmatrix} \begin{Bmatrix} \delta_1^{comp} \\ \delta_2 \\ \dots \\ \delta_m \end{Bmatrix} + \begin{Bmatrix} N_1 \\ 0 \\ \dots \\ 0 \end{Bmatrix} . \qquad (5.1)$$

where $\ddot{\delta}_1 = 0$ has been assumed and N_1 substitutes for the elastic force at point Q_1. The first row yields the contact force

$$N_1 = \begin{bmatrix} m_{12} & \dots & m_{1m} \end{bmatrix} \begin{Bmatrix} \ddot{\delta}_2 \\ \dots \\ \ddot{\delta}_m \end{Bmatrix} . \qquad (5.2)$$

while the remaining rows lead to the equation of the vibration problem:

$$\begin{bmatrix} m_{22} & \dots & m_{2m} \\ \dots & \dots & \dots \\ m_{m2} & \dots & m_{mm} \end{bmatrix} \begin{Bmatrix} \ddot{\delta}_2 \\ \dots \\ \ddot{\delta}_m \end{Bmatrix} + \begin{bmatrix} k_2 & & \\ & \dots & \\ & & k_m \end{bmatrix} \begin{Bmatrix} \delta_2 \\ \dots \\ \delta_m \end{Bmatrix} = \begin{Bmatrix} 0 \\ \dots \\ 0 \end{Bmatrix} \tag{5.3}$$

$$\Rightarrow \mathbf{M}'_n \ddot{\boldsymbol{\delta}}' + \mathbf{K}'_n \boldsymbol{\delta}' = \mathbf{0} \Rightarrow \mathbf{D}'_n = \left(\mathbf{M}'_n\right)^{-1} \mathbf{K}'_n \ .$$

Combining Eqs. (5.2) and (5.3), we obtain:

$$\begin{Bmatrix} \ddot{\delta}_2 \\ \dots \\ \ddot{\delta}_m \end{Bmatrix} = -\left(\mathbf{M}'_n\right)^{-1} \mathbf{K}'_n \begin{Bmatrix} \delta_2 \\ \dots \\ \delta_m \end{Bmatrix} \Rightarrow N_1 = -\begin{bmatrix} m_{12} & \dots & m_{1m} \end{bmatrix} \left(\mathbf{M}'_n\right)^{-1} \mathbf{K}'_n \begin{Bmatrix} \delta_2 \\ \dots \\ \delta_m \end{Bmatrix} \ . \tag{5.4}$$

There are four different possible situations:

- $\left(N_1^{comp} > N_1 > N_1^{exp}\right) \Rightarrow$ the constraint at Q_1 holds;
- $\left(N_1 > N_1^{comp}\right) \Rightarrow$ a new compression phase starts;
- $\left(N_1 < N_1^{exp}\right) \Rightarrow$ an expansion phase starts;
- $\left(N_1 < 0\right) \Rightarrow$ contact at Q_1 is lost.

This careful analysis is essential to properly define the inertia end stiffness matrices appearing in the motion equation (2.1). At every time step, Eq. (2.1) yields the position and velocity of all the impact points, $\boldsymbol{\delta}$ and $\dot{\boldsymbol{\delta}}$ respectively. In order to proceed one step further, the following analysis has to be done for each impact point Q_i (δ_{ni} will be used to denote the nth-permanent indentation associated with that point). According to the separating velocity $\dot{\delta}_i$, three different cases are defined to simplify the explanation.

CASE 1: $\dot{\delta}_i < 0$

if $\left(0 \le |\delta_i| \le |\delta_{ni}|\right)$

Compression of the upper spring: $k_i = k_i^{comp},\ N_i = k_i^{comp}\left|\delta_i - \delta_{ni}\right|,\ \mathbf{M}_n = \mathbf{M}_n$

elseif $\left(|\delta_i| > |\delta_{ni}|\right)$

Compression of the two springs: $k_i = k_i^{*comp},\ N_i = k_i^{*comp}\left|\delta_i\right|,\ \mathbf{M}_n = \mathbf{M}_n$

end

CASE 2: $\dot{\delta}_i = 0$

Calculate the constraint force to keep $\dot{\delta}_i = 0$**:** $N_i^{const} = -\left\{m_{ij}\right\}^T \left(\mathbf{M}_n'\right)^{-1} \mathbf{K}_n' \left\{\delta_{j\neq i}\right\}$

Calculate the expansion limit value: $N_i^{exp} = k_i^{exp}\left|\delta_i - \delta_{ni}\right|$

if $\left(0 \le |\delta_i| \le |\delta_{ni}|\right)$

Calculate the compression limit value: $N_i^{comp} = k_i^{comp}\left|\delta_i - \delta_{ni}\right|$

elseif $\left(|\delta_i| > |\delta_{ni}|\right)$

Calculate the compression limit value: $N_i^{comp} = k_i^{*comp}\left|\delta_i\right|$

end

if $\left(N_i^{const} > N_i^{comp}\right)$

Go to **CASE 1**

elseif $\left(N_i^{comp} > N_i^{const} > N_i^{exp}\right)$

The constraint holds: $\left(N_i = N_i^{const}\right),\ N_i = N_i^{const},\ \delta_{(n+1)i} = \delta_i,\ \mathbf{M}_n = \mathbf{M}_n'$

elseif $\left(N_i^{const} < N_i^{exp}\right)$

Go to **CASE 3**

elseif $\left(N_i^{const} < 0\right)$

Contact lost: $\left(N_i = 0\right),\ N_i = 0,\ \mathbf{M}_n = \mathbf{M}_n'$

end

CASE 3: $\dot{\delta}_i > 0$

if $\left(\delta_i = 0\right)$

Contact lost: $N_i = 0,\ \mathbf{M}_n = \mathbf{M}_n'$

elseif $\left(0 \le |\delta_i|\right)$

Expansion of the upper spring: $k_i = k_i^{exp},\ N_i = k_i^{exp}\left|\delta_i - \delta_{ni}\right|,\ \mathbf{M}_n = \mathbf{M}_n$

end

5.2 Exploration of transient constraints in a redundant multiple-point collision

As outlined in Section 2, it is necessary to choose a subset of independent colliding points when the system presents redundancy. The immediate consequence is that the stiffness matrix is not any more diagonal [1]. As the choice of independent colliding points may be changed along the problem, a contact point reaching the end of a compression phase, say Q_1, can always be taken as an independent point. At that time instant, $\dot{\delta}_1 = 0$ and $N_1^{comp} = -k_1^{comp}\delta_1$.

The investigation of a possible unilateral constraint at Q_1 parallels that presented for the nonredundant case. In equation $\tilde{\mathbf{M}}_n\ddot{\boldsymbol{\delta}}_n + \tilde{\mathbf{K}}_n\boldsymbol{\delta}_n = 0$, the constraint force N_1 substitutes for the elastic force $k_1\delta_1$ at point Q_1:

$$\begin{bmatrix} \tilde{m}_{11} & \tilde{m}_{12} & \dots & \tilde{m}_{1p} \\ \tilde{m}_{21} & \tilde{m}_{22} & \dots & \tilde{m}_{2p} \\ \dots & \dots & \dots & \dots \\ \tilde{m}_{m1} & \tilde{m}_{m2} & \dots & \tilde{m}_{pp} \end{bmatrix} \begin{Bmatrix} 0 \\ \ddot{\delta}_2 \\ \dots \\ \ddot{\delta}_p \end{Bmatrix} = -\begin{bmatrix} \tilde{k}_{11} & \tilde{k}_{12} & \dots & \tilde{k}_{1p} \\ \tilde{k}_{21} & \tilde{k}_{22} & \dots & \tilde{k}_{2p} \\ \dots & \dots & \dots & \dots \\ \tilde{k}_{m1} & \tilde{k}_{m2} & \dots & \tilde{k}_{pp} \end{bmatrix} \begin{Bmatrix} \delta_1^{comp} \\ \delta_2 \\ \dots \\ \delta_p \end{Bmatrix} + \begin{Bmatrix} N_1 \\ 0 \\ \dots \\ 0 \end{Bmatrix} . \tag{5.5}$$

From the first row:

$$N_1 = \begin{bmatrix} \tilde{m}_{12} & \dots & \tilde{m}_{1p} \end{bmatrix} \begin{Bmatrix} \ddot{\delta}_2 \\ \dots \\ \ddot{\delta}_p \end{Bmatrix} + \begin{bmatrix} \tilde{k}_{11} & \dots & \tilde{k}_{1p} \end{bmatrix} \begin{Bmatrix} \delta_1^{comp} \\ \dots \\ \delta_p \end{Bmatrix} . \tag{5.6}$$

The remaining rows lead to the equation of the vibration problem:

$$\begin{bmatrix} \tilde{m}_{22} & \dots & \tilde{m}_{2p} \\ \dots & \dots & \dots \\ \tilde{m}_{p2} & \dots & \tilde{m}_{pp} \end{bmatrix} \begin{Bmatrix} \ddot{\delta}_2 \\ \dots \\ \ddot{\delta}_p \end{Bmatrix} + \begin{bmatrix} \tilde{k}_{22} & \dots & \tilde{k}_{2p} \\ \dots & \dots & \dots \\ \tilde{k}_{p2} & \dots & \tilde{k}_{pp} \end{bmatrix} \begin{Bmatrix} \delta_2 \\ \dots \\ \delta_p \end{Bmatrix} = \begin{bmatrix} \tilde{k}_{21} \\ \dots \\ \tilde{k}_{p1} \end{bmatrix} \delta_1^{comp}$$

$$\Rightarrow \tilde{\mathbf{M}}_n'\ddot{\boldsymbol{\delta}}' + \tilde{\mathbf{K}}_n'\boldsymbol{\delta}' = \begin{bmatrix} \tilde{k}_{21} \\ \dots \\ \tilde{k}_{p1} \end{bmatrix} \delta_1^{comp} \tag{5.7}$$

According to Eq. (5.7), the system vibrates around the new equilibrium configuration:

$$\boldsymbol{\delta}^{eq} \equiv \begin{Bmatrix} \delta_2^{eq} \\ \dots \\ \delta_p^{eq} \end{Bmatrix} = \left(\tilde{\mathbf{K}}_n^{'}\right)^{-1} \begin{bmatrix} \tilde{k}_{21} \\ \dots \\ \tilde{k}_{p1} \end{bmatrix} \delta_1^{comp} \tag{5.8}$$

The corresponding dynamical matrix is $\tilde{\mathbf{D}}' = \left(\tilde{\mathbf{M}}_n^{'}\right)^{-1} \tilde{\mathbf{K}}_n^{'}$.

From the above equations:

$$\begin{Bmatrix} \ddot{\delta}_2 \\ \dots \\ \ddot{\delta}_p \end{Bmatrix} = -\left(\tilde{\mathbf{M}}_n^{'}\right)^{-1} \tilde{\mathbf{K}}_n^{'} \begin{Bmatrix} \delta_2 \\ \dots \\ \delta_p \end{Bmatrix} + \left(\tilde{\mathbf{M}}_n^{'}\right)^{-1} \begin{bmatrix} \tilde{k}_{21} \\ \dots \\ \tilde{k}_{p1} \end{bmatrix} \delta_1^{comp} \ , \tag{5.9}$$

and, consequently:

$$N_1 = -\begin{bmatrix} \tilde{m}_{12} & \dots & \tilde{m}_{1p} \end{bmatrix} \left(\tilde{\mathbf{M}}_n^{'}\right)^{-1} \left(\tilde{\mathbf{K}}_n^{'} \begin{Bmatrix} \delta_2 \\ \dots \\ \delta_p \end{Bmatrix} + \begin{bmatrix} \tilde{k}_{21} \\ \dots \\ \tilde{k}_{p1} \end{bmatrix} \delta_1^{comp} \right) + \begin{bmatrix} \tilde{k}_{11} & \tilde{k}_{12} & \dots & \tilde{k}_{1p} \end{bmatrix} \begin{Bmatrix} \delta_1 \\ \delta_2 \\ \dots \\ \delta_p \end{Bmatrix} \tag{5.10}$$

6 APPLICATION EXAMPLES

The main purpose of the application examples is to illustrate a variety of situations (different sequences of compressions and expansions, with or without creation of unilateral constraints). Thus, we will not be presenting complicated systems but mainly two examples of planar impacts (for the sake of clarity in the analysis of results) with different elastoplastic conditions. Each simulation is carried out until all colliding points reach either a state of unilateral constraint or start a "free" motion (that is, do not touch the ground).

6.1 Example I

The first example consists on a two-point impact of a rod on a fixed ground (Fig.9). The mass (1 kg) is concentrated on half of its length (that is, along 2 m), and the contact points Q_1 and Q_2 are located at the rod ends. The initial configuration is always that of Fig.9, and the

initial motion is always a vertical translation (so the initial velocity at the colliding points is the same and equal to 1 m/s).

As a reference case, Fig.10 shows the result for a ground with equal elastoplastic characteristics at both points Q_1 and Q_2: a same value of 10^3 kN/m for k and k′, and no dissipation associated with the upper set (that is, $\mu = 0$). In this case, then, $k^{comp} = k^{exp} = k$ and $k^{*comp} = 2k'$. As no pre-compression has been assumed ($N_0 = 0$), both springs are deforming from the very beginning, and the total equivalent stiffness is that given in Eq. (3.1). The initial equilibrium configuration is

$$\left(\boldsymbol{\delta_0^{eq}}\right)^T = \{0 \quad 0\} = \left\{\delta_0^{eq}(Q_1) \quad \delta_0^{eq}(Q_2)\right\} = \{0 \quad 0\} \tag{6.1}$$

Whenever a point Q_i reaches a local maximum compression (that is, a zero approaching velocity) within a zone where both springs are deforming, the irreversible deformation (new equilibrium position) $\delta^{eq}(Q_i)$ and the force interval allowed for the potential constraint force $\left[N_i^{comp}, N_i^{exp}\right]$ are calculated. As $\mu = 0$ in the present case, $N_i^{comp} = N_i^{exp} \equiv N_i$, so the colliding points will never be constrained. The end of a compression phase will imply systematically the beginning of an expansion phase.

If a local maximum compression is reached without further deforming the lower spring, the equilibrium configuration does not change, and so no new $\delta^{eq}(Q_i)$ has to be calculated.

Four different plots are presented for each colliding point: $\delta(t)$ -upper left-, $\dot{\delta}(t)$ -upper right-, $N(t)$ -lower left- and $N(\delta)$ -lower right-. Fig.10(a)-(d) correspond to point Q_1 and Fig.10(e)-(h) correspond to point Q_2. The successive $\delta^{eq}(Q_i)$ configurations are indicated in red in plots (a,d) –point Q_1– and (e,h) –point Q_2 -.

Point Q_1 motion shows three different phases:

- $[0, t_a]$: two-spring compression (with k^{*comp});

- $[t_a, t_b]$: one-spring expansion (with k^{exp}); the lower spring remains compressed with $N_a = k'\left|\delta_1^{eq}(Q_1)\right|$; the new equilibrium configuration $\delta_1^{eq}(Q_1)$ is calculated through $k^{*comp}\delta_1(t_a) = k^{exp}\left(\delta_1(t_a) - \delta_1^{eq}(Q_1)\right)$.

- $[t_b, t_c]$: as $\left|\delta_1(t_b)\right| = \left|\delta_1^{eq}(Q_1)\right|$ and $\dot{\delta}_1(t_b) > 0$, point Q_1 does not touch the ground and so undergoes a "free" motion.

Point Q_2 motion is more complicated. Up to seven phases can be distinguished:

- $[0, t_a]$: two-spring compression (with k^{*comp}); new equilibrium configuration with $\delta_1^{eq}(Q_2) = \left(1 - \left(k^{*comp}/k^{exp}\right)\right)\delta_2(t_a)$ and lower spring compression force $N_a = k'\left|\delta_1^{eq}(Q_2)\right|$.

- $[t_a, t_b]$: one-spring expansion (with k^{exp});

- $[t_b, t_c]$: one-spring compression (with k^{comp}); when the total compression force associated with the upper spring reaches the value N_a, the lower spring will start a compression phase if $\dot{\delta}_2 < 0$.

- $[t_c, t_d]$: two-spring compression (k^{*comp}); new equilibrium configuration with $\delta_2^{eq}(Q_2) = \left(1 - \left(k^{*comp}/k^{exp}\right)\right)\delta_2(t_d)$ and lower spring compression force $N_d = k'\left|\delta_2^{eq}(Q_2)\right|$;

- $[t_d, t_e]$: one-spring expansion (k^{exp});

- $[t_e, t_f]$: one-spring compression (k^{comp}); as the total contact force for $t = t_f$, $k^{comp}\left|\delta_2(t_f) - \delta_2^{eq}(Q_2)\right|$, is lower than the compression force of the lower spring (N_d), an expansion phase will start;

- $\left[t_f, t_g\right]$: one-spring expansion (k^{exp}); as $\delta_2\left(t_g\right) = \delta_2^{eq}\left(Q_2\right)$ and point Q_1 is moving upwards, no new compressions will take place and so the collision is over.

The previous analysis is summarized in Table I. In order to facilitate the description of the results, the analysis of the motion phases for the following examples will be directly given in Tables, and a few comments will be explicitly commented.

Table I

Point	Phase interval	Description	Equilibrium configuration	Lower spring compression force
Q_1	$[0, t_a]$	Two-spring compression $\left(k^{*comp}\right)$	$\delta_0^{eq}(Q_1) = 0$	0
	$[t_a, t_b]$	One-spring expansion $\left(k^{exp}\right)$	$\delta_1^{eq}(Q_1) = \left(1 - \frac{k^{*comp}}{k^{exp}}\right)\delta_1(t_a)$	$N^{low}(Q_1) \le N_a$ $N_a = k'\left\|\delta_1^{eq}(Q_1)\right\|$
	$[t_b, t_c]$	No ground contact		
Q_2	$[0, t_a]$	Two-spring compression $\left(k^{*comp}\right)$	$\delta_0^{eq}(Q_2) = 0$	0
	$[t_a, t_b]$	One-spring expansion $\left(k^{exp}\right)$	$\delta_1^{eq}(Q_2) = \left(1 - \frac{k^{*comp}}{k^{exp}}\right)\delta_2(t_a)$	$N^{low}(Q_2) \le N_a$ $N_a = k'\left\|\delta_1^{eq}(Q_2)\right\|$
	$[t_b, t_c]$	One-spring compression $\left(k^{comp}\right)$		
	$[t_c, t_d]$	Two-spring compression $\left(k^{*comp}\right)$		
	$[t_d, t_e]$	One-spring expansion $\left(k^{exp}\right)$	$\delta_2^{eq}(Q_2) = \left(1 - \frac{k^{*comp}}{k^{exp}}\right)\delta_2(t_d)$	$N^{low}(Q_2) \le N_d$ $N_d = k'\left\|\delta_2^{eq}(Q_2)\right\|$
	$[t_e, t_f]$	One-spring compression $\left(k^{comp}\right)$		
	$[t_f, t_g]$	One-spring expansion $\left(k^{exp}\right)$		

Two variations on that example are shown in Figs.11 and 12. The first one consists on adding some friction on the upper sets associated with both points: $\mu_1 = \mu_2 = 0.1$. As there is no pre-compression, $\left(\boldsymbol{\delta}_{\mathbf{0}}^{\mathbf{eq}}\right)^{\mathrm{T}} = \{0 \quad 0\}$.

The plots in Figs.11(a)-(d) correspond to point Q_1. The main difference, as compared to the reference case (Figs.10(a)-(d)), is the sudden decrease of the normal force in transition from compression to expansion, associated to the nonzero friction added to that point. That discontinuity is clearly observed on plots (c) and (d): $\Delta N = N_b^{exp} - N_a^{comp} < 0$. Besides that, point Q_1 motion shows the same three different phases as before: two-spring compression, one-spring expansion, "free" motion.

Point Q_2 motion is again more complicated. Whereas in the reference case (Figs.10(e)-(h)) its motion was a succession of three continuous compression-expansion phases, in the present case there are only two compression-expansion phases showing a normal force discontinuity at each transition (compression to expansion, expansion to compression) associated to the upper spring nonzero friction coefficient. Starting with an equilibrium configuration with zero deformation, point Q_2 undergoes two irreversible indentations leading to two nonzero equilibrium deformations.

The second and last variation (Fig.12) consists of considering a nonzero friction on the upper set associated with point Q_2, $\mu_2 = 0.3$, and a pre-compression at that same point $\left(\boldsymbol{\delta}_{\mathbf{0}}^{\mathbf{eq}}\right)^{\mathrm{T}} = \{0 \quad -0.1\,\mathrm{mm}\}$.

The plots in Figs.12(a)-(d) correspond to point Q_1. Having a zero friction on its upper set leads to results which are qualitatively identical to those of the reference case, and so no further comments are necessary.

Point Q_2 motion (Figs.12(e)-(h)) is much richer. The new feature (as compared to the previous cases) is the existence of unilateral constraint phases (that is, phases where point Q does not move though its associated normal force varies between two limits).

Eight different phases (compression, expansion, constraint) can be distinguished. Their description is summarized in Table II.

Table II (point Q_2)

Phase interval	Short description	Equilibrium configuration
$[0, t_a]$	One-spring compression $\left(k^{comp}\right)$	$\delta_0^{eq}(Q_2) = 0.1\,\text{mm}$
	As the lower set is already pre-compressed, the upper set undergoes a compression phase until its associated repulsion force equals the lower pre-compression $\left(N_a^{comp}\right)$.	
$[t_a, t_b]$	Two-spring compression $\left(k^{*comp}\right)$	$\delta_0^{eq}(Q_2) = 0.1\,\text{mm}$
	The normal force is higher than the initial pre-compression $\left(N_a^{comp}\right)$, and so both springs undergo a compression phase until reaching an instantaneous zero velocity $\dot{\delta}_2(t_b) = 0$. The lower set will remain compressed and will not undergo a new compression until the normal force reaches the value N_b^{comp}.	
$[t_b, t_d]$	One-spring expansion $\left(k^{exp}\right)$	$\delta_1^{eq}(Q_2) = \left(1 - \dfrac{k^{*comp}}{k^{exp}}\right)\delta_2(t_a)$
	Expansion starts, but having a nonzero friction $(\mu = 0.3)$, a sudden decrease in the normal force appears; expansion goes on until reaching an instantaneous zero velocity $\dot{\delta}_2(t_d) = 0$. If a compression started immediately after, there would be a sudden increase in the normal force $\Delta N = N_e^{comp} - N_d^{exp} > 0$.	
$[t_d, t_e]$	Unilateral constraint	$\delta_1^{eq}(Q_2) = \left(1 - \dfrac{k^{*comp}}{k^{exp}}\right)\delta_2(t_a)$
	The calculation of the force needed to keep the zero separation velocity falls within the range $\left[N_d^{exp}, N_e^{comp}\right]$. Thus, the normal force adapts its value and the unilateral constraint is maintained until its value falls out of the allowed range.	
$[t_e, t_f]$	One-spring compression $\left(k^{comp}\right)$	$\delta_1^{eq}(Q_2) = \left(1 - \dfrac{k^{*comp}}{k^{exp}}\right)\delta_2(t_a)$

	The normal force reaches the value N_e^{comp}, so the unilateral constraint is lost and a new compression phase starts. As $N_e^{comp} < N_b^{comp}$, it is only the upper-spring the one undergoing deformation.	
$[t_f, t_g]$	Two-spring compression (k^{*comp})	$\delta_1^{eq}(Q_2) = \left(1 - \frac{k^{*comp}}{k^{exp}}\right)\delta_2(t_a)$
	The normal force reaches the value N_b^{comp} but the separation velocity has not yet reached a zero value, so compression goes on but deforming both springs until reaching an instantaneous zero velocity $\dot{\delta}_2(t_f) = 0$.	
$[t_g, t_h]$	Unilateral constraint	$\delta_2^{eq}(Q_2) = \left(1 - \frac{k^{*comp}}{k^{exp}}\right)\delta_2(t_f)$
	The calculation of the force needed to keep the zero separation velocity falls within the range $\left[N_h^{exp}, N_g^{comp}\right]$. Thus, the normal force adapts its value (in this case, decreases) and the unilateral constraint is maintained until its value falls out of the allowed range.	
$[t_h, t_i]$	One-spring expansion (k^{*comp})	$\delta_2^{eq}(Q_2) = \left(1 - \frac{k^{*comp}}{k^{exp}}\right)\delta_2(t_f)$
	New expansion of the upper spring until the normal force reaches a zero value, indicating the end of the collision.	

6.2 Example II

The second example is a two-body system (Fig.13) consisting of two identical rods connected through a perfect hinge undergoing a two-point collision with the ground. The colliding points are located as shown in the upper part of Fig.13. Point Q_1 has neither upper-set friction nor lower-set initial pre-compression, while point Q_2 has a nonzero friction associated with the upper set and a lower-set initial pre-compression of 0.2 mm.

This application case has been included in order to check the validity of the model in multibody systems. The detailed sequence of compression and expansion phases can be seen on Figs.13(a)-(d) for point Q_1 and on Figs.13(e)-(h) for point Q_2. Point Q_1 shows just a

compression, an expansion phase and then a contact loss. Collision at point Q_2 is composed of two upper-spring compressions and two upper-spring expansions. No simultaneous deformation of the two sets is observed.

7. CONCLUSIONS

We presented a model concerning the normal interaction between colliding bodies. Our work encompasses three different aspects:

- the number of simultaneously colliding points is not limited, as our model deals efficiently with kinematical redundancy;
- the approach intrinsically considers the possibility of a variable number of DoF associated with creation or loss of unilateral constraints during the collision interval; unilateral constraints are thereby systematically inspected;
- the model covers the whole range of energy dissipation hypothesis: from perfectly elastic to totally plastic, going through all possible degrees of inelasticity and permanent indentations.

The two first aspects were previously addressed in [1]. The third one is entirely new and is based on a constitutive viscoelastic model for the normal behaviour of the colliding bodies based on a simple arrangement of two elementary sets of springs and dry-friction dampers. The first set accounts for inelastic behavior (i.e., energy loss with no permanent deformation), while the second one introduces a component of plastic behavior (i.e., energy dissipation with permanent deformation). The model parameters were tuned through comparison with several examples from the scientific literature. In all cases, it yields dynamically consistent results.

Future work will consist in adding tangential properties to the colliding bodies (roughness, tangential compliance).

REFERENCES

[1] Barjau, A., Batlle, J.A. & Font-Llagunes, J.M. : Combining vibrational linear-by-part dynamics and kinetic-based decoupling og the dynamics for multiple smoothimpacts with redundancy, Multibody Syst. Dyn, 31, 1-21 (2013) (DOI 10.1007/s11044-013-9398-z)

[2] Stronge, W.J. : Impact mechanics. Cambridge University Press (2000) (doi: http://dx.doi.org/10.1017/CBO9780511626432)

[3] Brogliato, B. : Nonsmooth Mechanics. Models, Dynamics and Control. Springer, 2nd edition (1999)

[4] W. Schiehlen, R. Seifried & P. Eberhard, Elastoplastic phenomena in multibody impact dynamics, Comput. Methods Appl. Mech. Eng., 195, 6874-6890, (2006) (DOI 10.1016/j.cma.2005.08)

[5] Glocker, C.: Energetic consistency conditions for standard impacts. Part I: Newton-type inequality laws and Kane's example. Multibody Syst. Dyn. 29, 77-117 (2013)

[6] Batlle, J.A. : Termination conditions for three-dimensional inelastic collisions in multibody systems, Int. J. Impact Eng. 25(7), 615-629 (2001) (DOI: 10.1016/S0734-743X(01)00007-0)

[7] AgulloBatlle, J. & Barjau, A. : Rough impacts in multibody systems, Mech. And Mach. Theory, 26(6), 565-577 (1991) (DOI 10.1016/0094-114X(91)90039-7)

[8] Ivanov, A.P. : On multiple impact. J. Appl. Maths. Mechs. 59(6), 887-902 (1995)

[9] Liu, C., Zhao, Z. & Brogliato, B. : Frictionless multiple impacts in multibody systems. Part I: Theoretical framework, Proc. R. Soc. A, Math. Phys. Eng. Sci. 465(2101), 3193-3211 (2008)

[10] Nguyen, N.S. & Brogliato, B. : Multiple Impacts in Dissipative Granular Chains, Springer-Verlag (2014)

[11] Wang, J., Liu, C. & Zhao, Z.: Nonsmooth dynamics of a 3D rigid body on a vibrating plate. Multibody Syst. Dyn. 32, 217-239 (2014)

[12] Ruspini, D.C. & Khatib, O. : Impact/Contact models for the dynamic simulation of complex environments, Proc. IEEE/RSJ Int. Conf. on Intelligent Robots and Systems, (1997)

[13] Johansson, L. : A Newton method for rigid body frictional impact with multiple simultaneous impact points, Computer Methods in Applied Mechanics and Engineering, 191, 239-254 (2001) (DOI 10.1016/S0045-7825(01)00272-9)

[14] Seifried, R.; Schiehlen, W. & Eberhard, P. : Numerical and experimental evaluation of the coefficient of restitution for repeated impacts. Int. J. Impact Eng., 32, 508-524 (2005) (DOI 10.1016/j.ijimpeng.2005.01.001)

[15] Wu, C.; Li, L. & Thornton, C. : Rebound behavior of spheres for plastic impacts. Int. J. Impact Eng., 28, 929-946 (2003) (DOI 10.1016/S0734-743X(03)00014-9)

[16] Biot, M.A. : Theory of Stress-Strain Relations in Anisotropic Viscoelasticity and Relaxation Phenomena, J. App. Phys. 25(2), 1385-1391 (1954)

[17] Johnson, K.L. : Contact Mechanics; Cambridge University Press, Cambridge, 1985.

[18] Hunt, K.H. & Crossley, F.R.E. : Coefficient of restitution interpreted as damping in vibroimpact, J. Appl. Mech. 42, 440-445 (1975)

[19] Lankarani, H.M. & Nikravesh, P.E. : Continuous contact force models for impact analysis in multi-body systems. Nonlinear Dyn. 5, 193-207 (1994)

[20] Flores, P., Machado, M., Silva, M.T. & Martins, J.M. : On the continuous contact force models for soft materials in multibody dynamics, Multibody Syst. Dyn. 25, 357-375 (2011)

[21] Walton, O.R. & Braun, R.L. : Stress Calculations for Assemblies of Inelastic Spheres in Uniform Shear, Acta Mechanica 63, 73-86 (1986a)

[22] Walton, O.R. & Braun, R.L. : Viscosity, granular temperature, and stress calculations for shearing assemblies of inelastic, frictional disks, J. Rheol. 30, 949-980 (1986b) (doi: http://dx.doi.org/10.1122/1.549893)

[23] Stronge, W.J. : Chain reaction from impact on aggregate of elasto-plastic 'rigid' bodies. Int. J. Impact Eng. 28, 291-302 (2003)

[24] Kruggel-Emden, H., Simsek, E., Rickelt, S., Wirtz, S. & Scherer, V. : Review and extension of normal force models for the Discrete Element Method, Powder Tech. 171, 157-173 (2007)

[25] Yigit, A.S. & Christoforou, A.P. : On the impact of a spherical indenter and an elastic-plastic transversely isotropic half-space. Compos. Eng. 4(11), 1143-1152 (1994)

[26] Vu-Quoc, LO. & Zhang, X. : An elastoplastic contact force-displacement model in the normal direction: displacement-driven version. Proc. R. Soc. Lond. A 455, 4013-4044 (1999)

[27] Sivaselvan, M.V. & Reinhorn, A.M. : Hysteretic models for deteriorating inelastic structures. J. Eng. Mech. 126(6), 633-640 (2000)

[28] Bastien, J. & Lamarque, C-H. : Persoz's gephyroidal model described by a maximal monotone differential inclusion. Arch. Appl. Mech. 78, 393-407 (2008)

[28] Bastien, J., Schatzman, M. & Lamarque, C-H. : Study of some rheological models with a finit number of degrees of freedom. Eur. J. Mech. A/Solids 19, 277-307 (2008)

[30] Ismail, M., Okhouane, F. & Rodellar, J. : The Hysteresis Bouc-Wen Model, a Survey. Arch. Comput. Methods Eng. 16, 161-188 (2009)

[31] Yigit, A.S, Christoforou, A.P. & Majeed, M.A. : A nonlinear visco-elastoplastic impact model and the coefficient of restitution. Nonlinear Dyn. 66, 509-521 (2011)

FIGURE CAPTIONS

Figure 1: (a) Elementary viscoelastic system consisting of a linear spring and a dry-friction damper. (b) Total force generated by the elementary system as a function of the deformation x (case $0<\mu<1$).

Figure 2: Total force generated by the elementary system as a function of the deformation x for the two extreme cases: (a) perfectly elastic system ($\mu=0$), no energy dissipation, no permanent deformation; (b) perfectly plastic system ($\mu=1$), energy dissipation (equal to the area of the shaded zone), nonzero permanent deformation.

Figure 3: Total force generated by the elementary system as a function of the deformation x for the general case $0<\mu<1$. (a) complete cycle compression-expansion, no permanent indentation, nonzero energy dissipation; (a) two compression-partial expansion cycles, no permanent indentation, nonzero energy dissipation.

Figure 4: Viscoelastic model consisting of two series elementary systems, the upper one with friction coefficient $0\le\mu<1$ (inelastic system), and the lower one with $\mu'=1$ (plastic system). Their deformation is defined through the absolute coordinates x and x_0, respectively. The plastic system cannot undergo expansion, and allows a force range $[0, 2k'x_0]$ at the midpoint.

Figure 5: Possible scenarios when using the viscoelastic series model. (a) From a zero initial indentation, the system undergoes a compression (AA') deforming both elementary systems, followed by an expansion phase (A"B) affecting only the upper system while the lower one remains deformed. (b) From the permanent deformation generated in scenario (a), the system undergoes a one-spring compression which may reach the limit value for which the lower system starts compressing (BA'), or end before it attains that value (BB'); new compressions of the plastic system are responsible for an increase of the permanent deformation.

Figure 6: Simulation of a ball-ground inelastic single-point collision. Indentation (a) and approaching velocity (b) along the impact interval for different values of the friction coefficient. The time scale has been normalized to that of the most dissipative case $(e=0.2)$. (c) Contact force as a function of the indentation.

Figure 7: Simulation of a ball-ground plastic single-point collision for two different sets of elastoplastic parameters and two different impact velocities. (a) equal upper and lower stiffness, 0.1 m/s impact velocity; (b) upper stiffness higher than the lower one, 1 m/s impact velocity.

Figure 8: Simulation of a succession of ball-ground plastic single-point collisions. The plot shows the evolution along the impact interval of the contact force for the first 10 collisions. The impact interval duration has been normalized to that of the first collision.

Figure 9: Two-point impact of a rod with a fixed ground. The rod mass is concentrated on its first half.

Figure 10: Evolution of normal displacement $\delta_n(t)$, separating velocity $\dot{\delta}_n(t)$, normal contact force $N(t)$ in and contact force *versus* indentation $N(|\delta_n|)$, in a simultaneous two-point impact of the rod in Fig.9 for the case of pure downwards translation. Plots (a)-(d) correspond to point Q_1, plots (e)-(h) to point Q_2. Zero initial precompression, zero friction in the upper set of the viscoelastic model.

Figure 11: Evolution of normal displacement $\delta_n(t)$, separating velocity $\dot{\delta}_n(t)$, normal contact force $N(t)$ in and contact force *versus* indentation $N(|\delta_n|)$, in a simultaneous two-point impact of the rod in Fig.9 for the case of pure downwards translation. Plots (a)-(d) correspond to point Q_1, plots (e)-(h) to point Q_2. Zero initial precompression, nonzero friction in the upper set of the viscoelastic model.

Figure 12: Evolution of normal displacement $\delta_n(t)$, separating velocity $\dot{\delta}_n(t)$, normal contact force $N(t)$ in and contact force *versus* indentation $N(|\delta_n|)$, in a simultaneous two-point impact of the rod in Fig.9 for the case of pure downwards translation. Plots (a)-(d) correspond to point Q_1, plots (e)-(h) to point Q_2. Nonzero initial precompression in both points, zero and nonzero friction in the upper set of the viscoelastic model for points Q_1 and Q_2, respectively.

Figure 13: Evolution of normal displacement $\delta_n(t)$, separating velocity $\dot{\delta}_n(t)$, normal contact force $N(t)$ in and contact force *versus* indentation $N(|\delta_n|)$, in a simultaneous two-point impact of an homogeneous rod for the case of pure downwards translation. Plots (a)-(d) corre-

spond to point Q_1, plots (e)-(h) to point Q_2. Nonzero initial precompression at point Q_2, zero and nonzero friction in the upper set of the viscoelastic model for points Q_1 and Q_2, respectively.

colour figure
Click here to download colour figure: Fig 1.eps

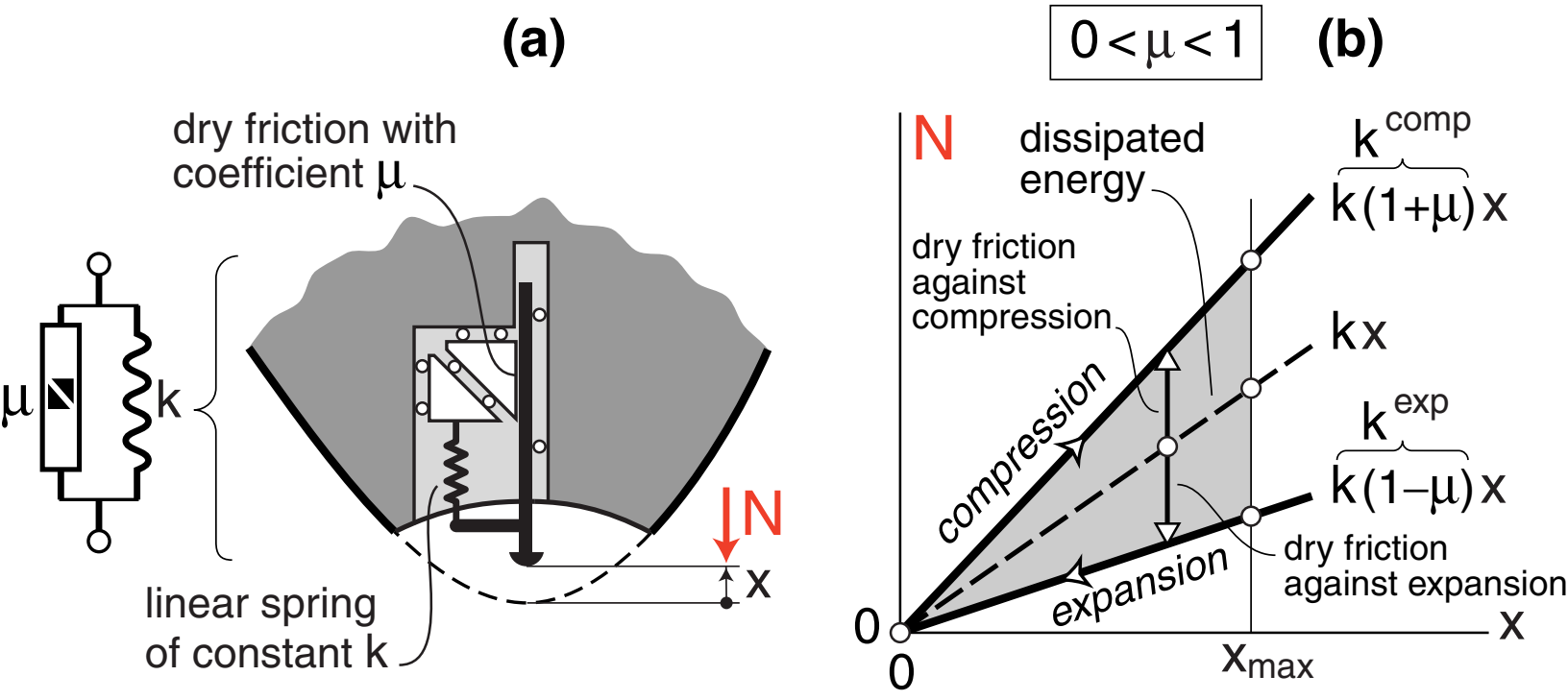

colour figure
Click here to download colour figure: Fig 2.eps

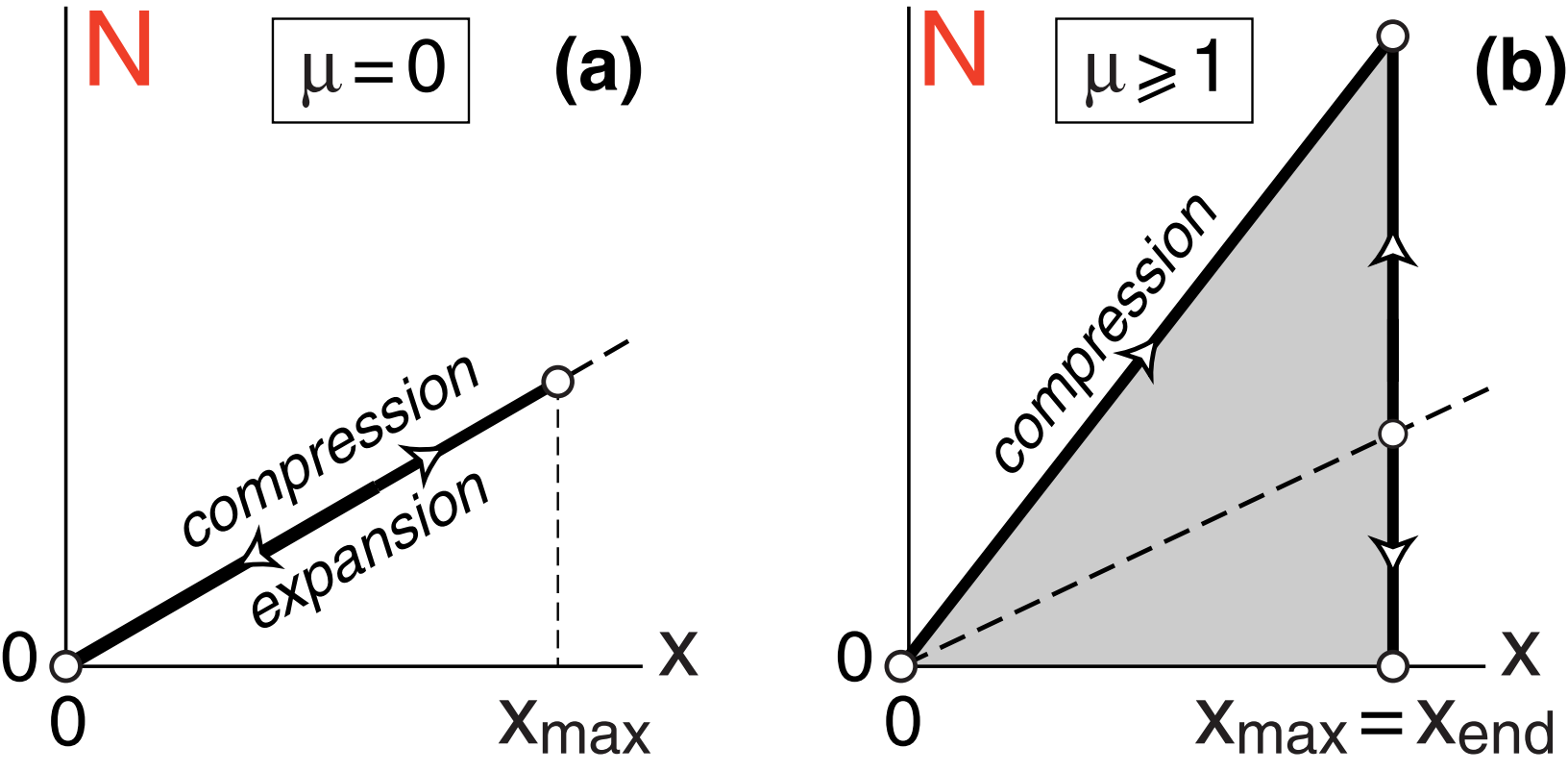

colour figure
Click here to download colour figure: Fig 3.eps

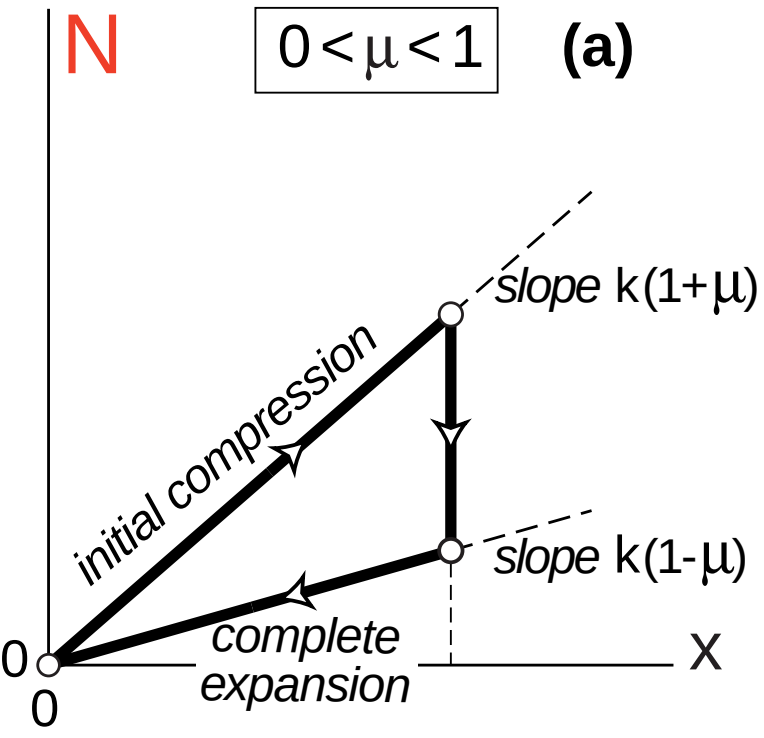

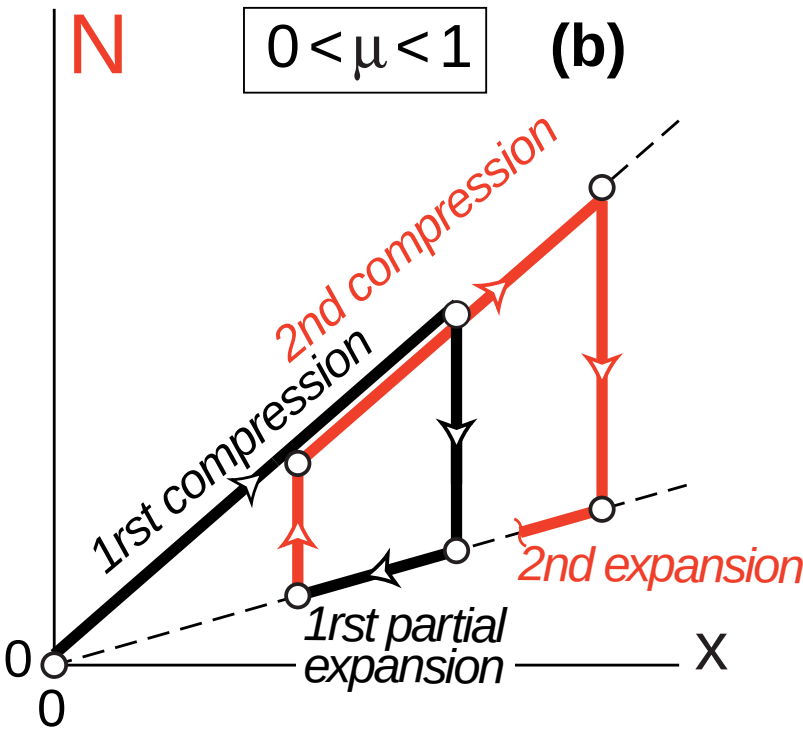

colour figure
Click here to download colour figure: Fig 4.eps

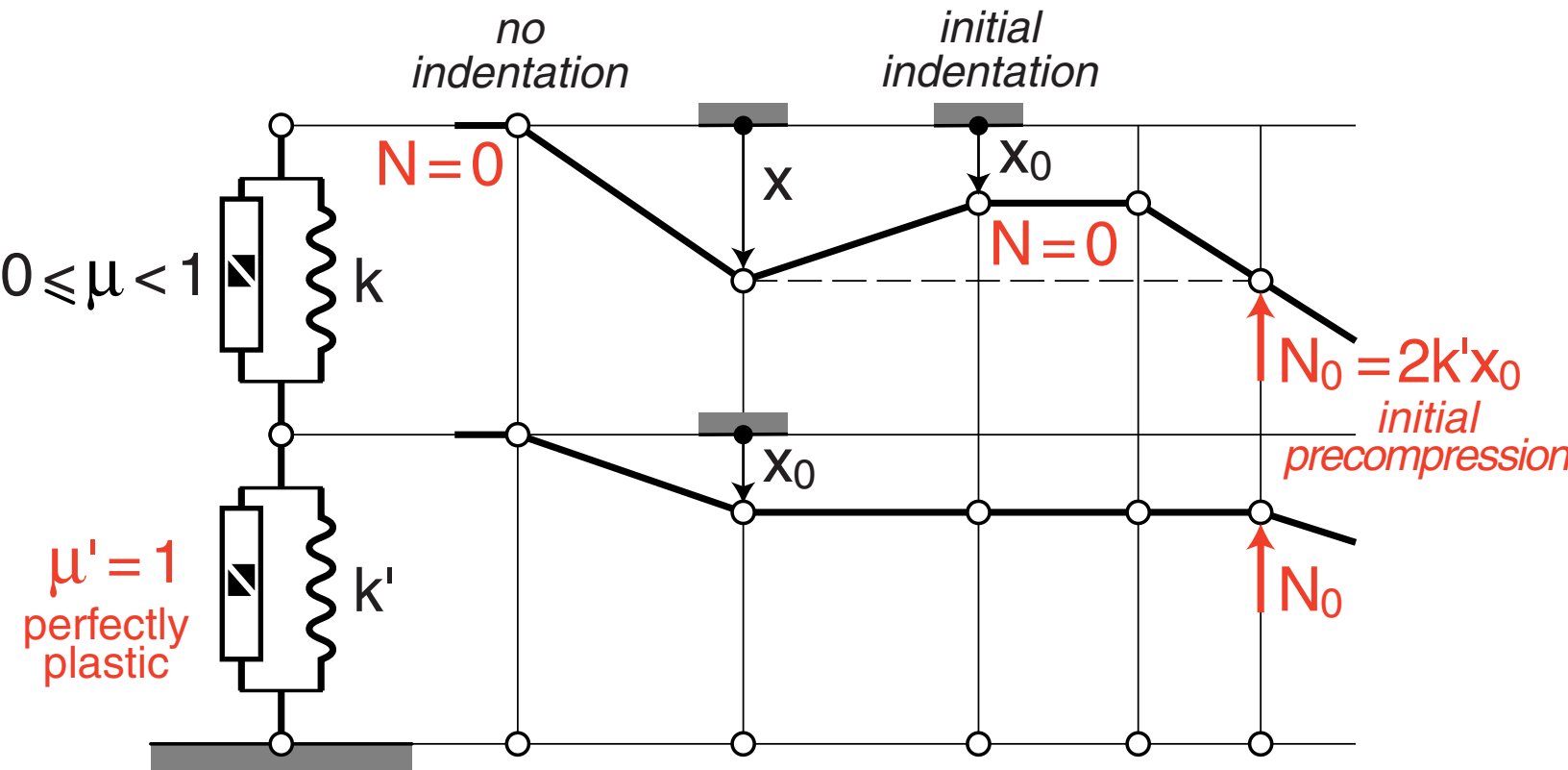

colour figure
Click here to download colour figure: Fig 5.eps

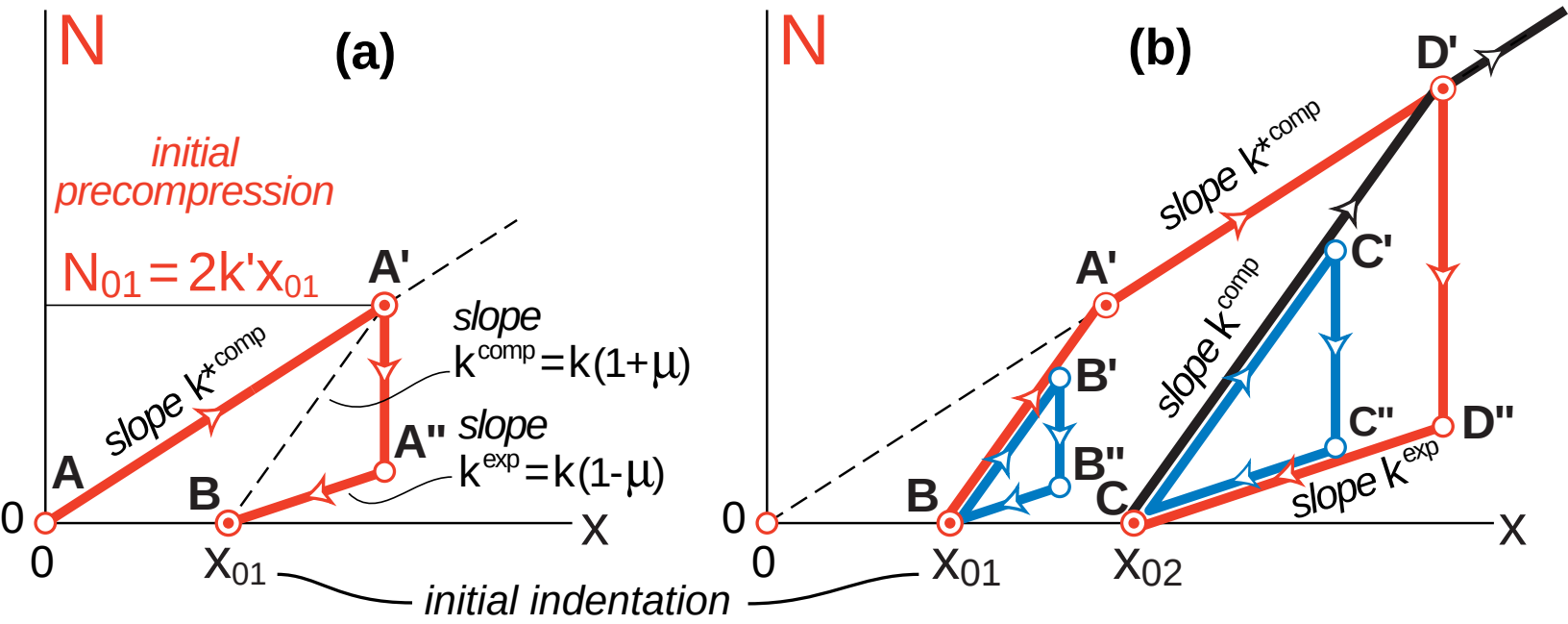

colour figure
Click here to download colour figure: Fig 6.eps

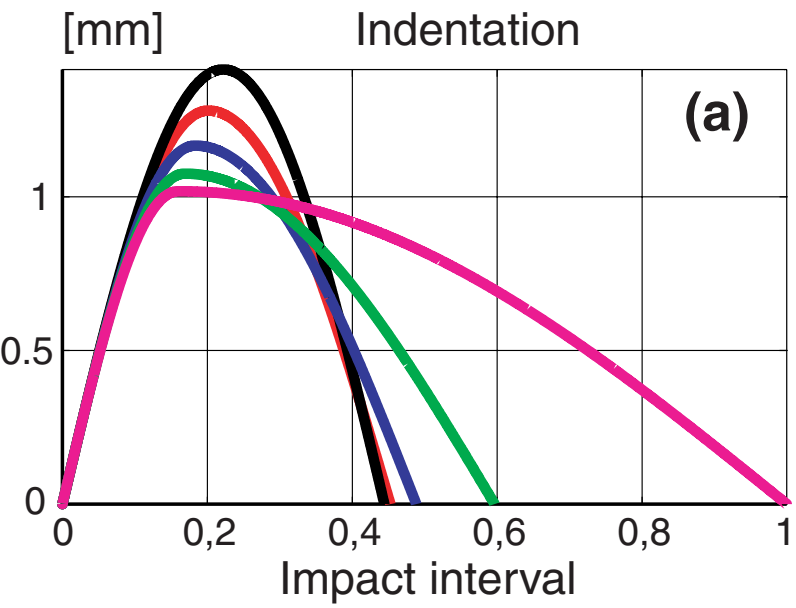

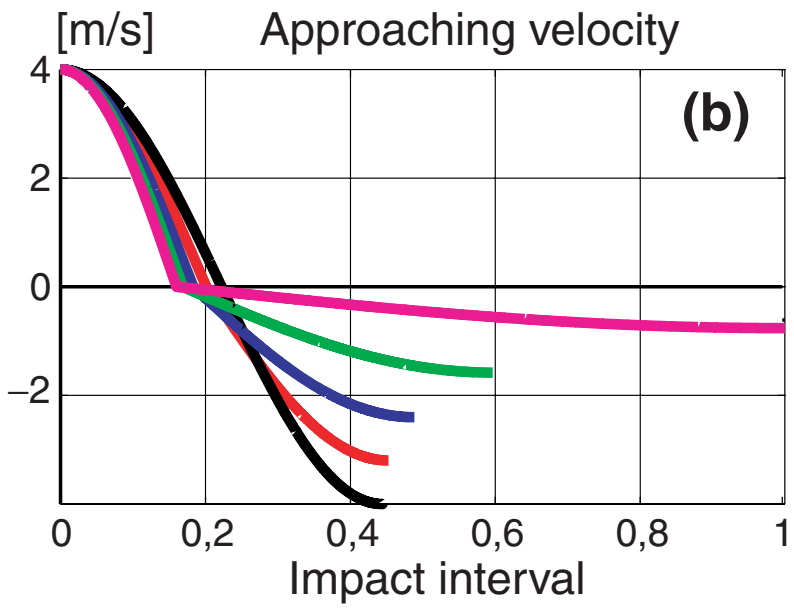

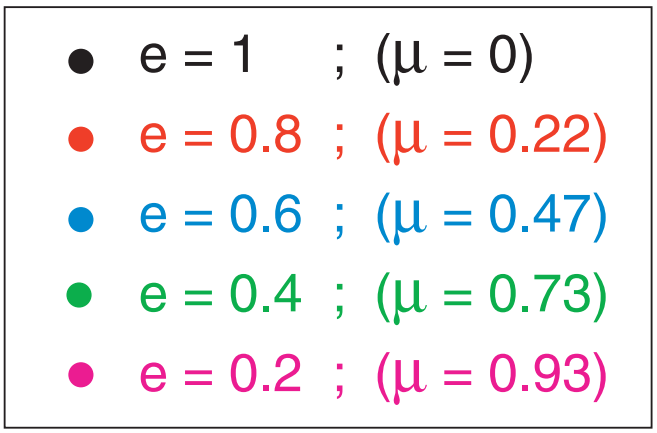

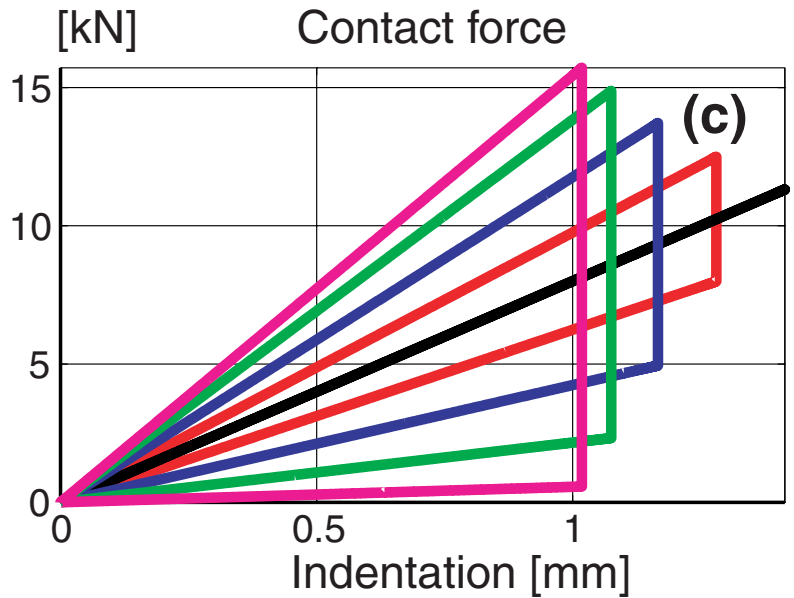

colour figure
Click here to download colour figure: Fig 7.eps

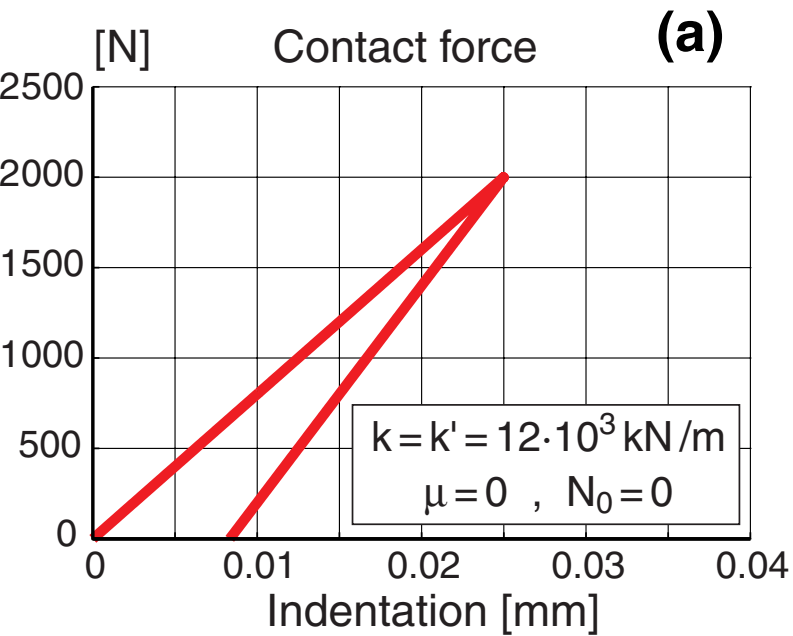

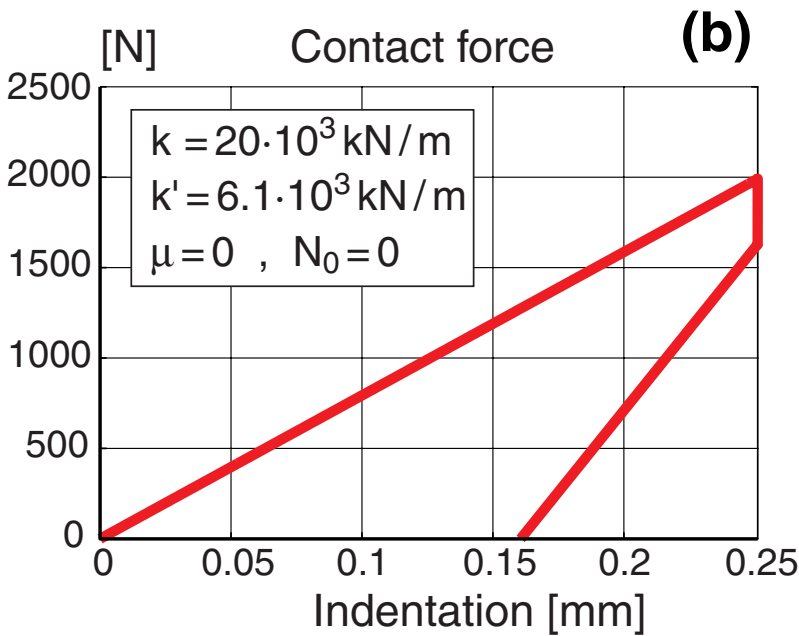

colour figure
Click here to download colour figure: Fig 8.eps

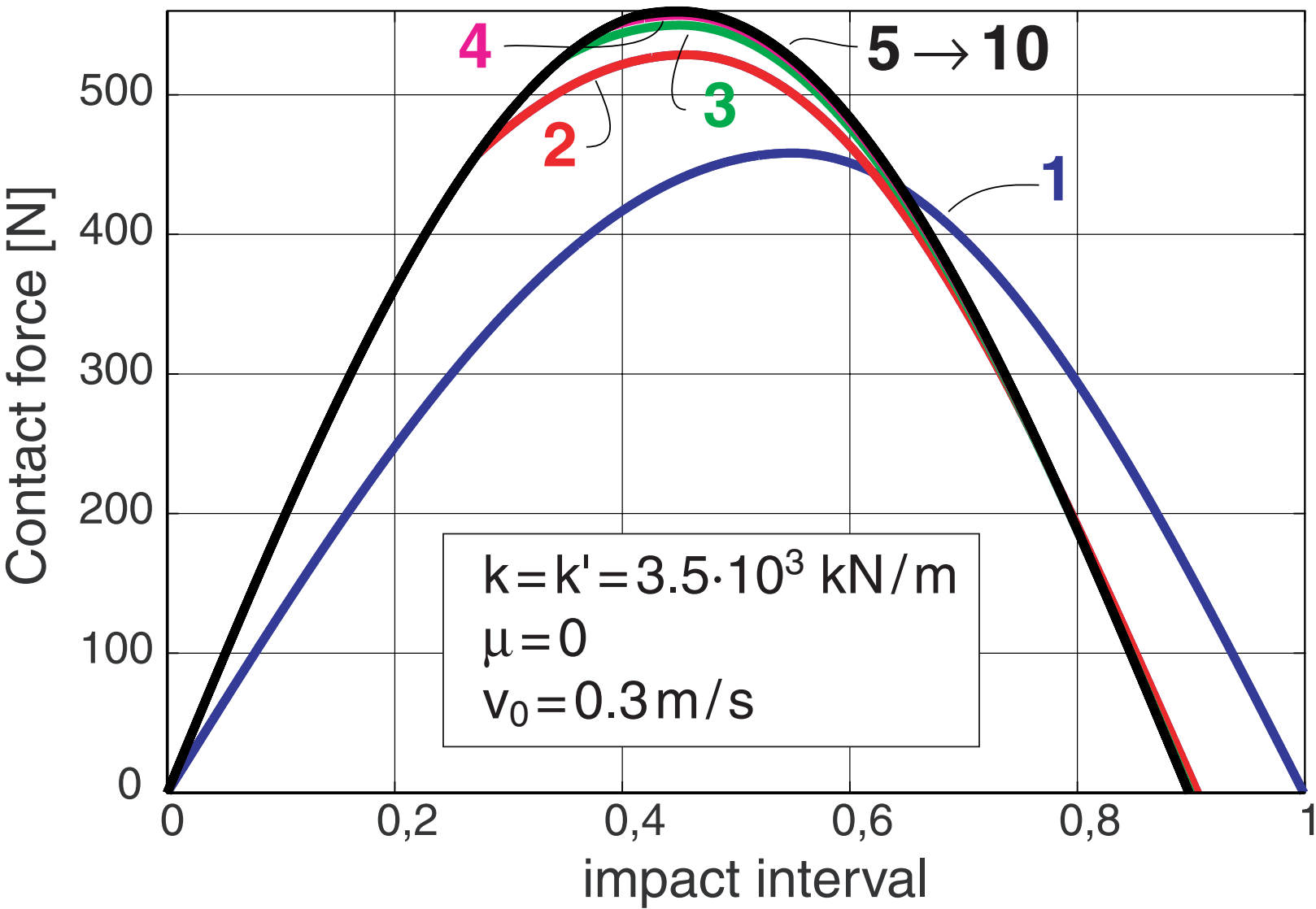

colour figure
Click here to download colour figure: Fig 9.eps

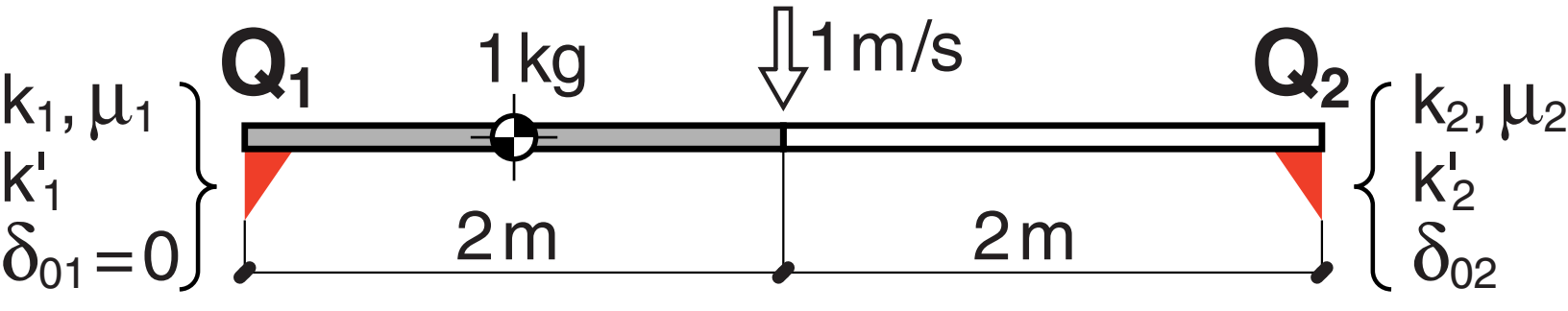

colour figure
Click here to download colour figure: Fig 10.eps

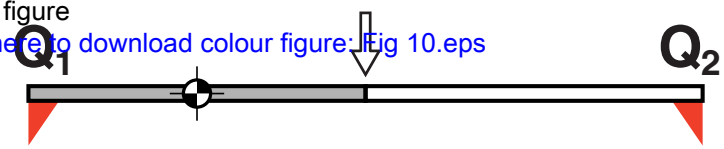

$k_1 = k_2 = k'_1 = k'_2 = 10^3$ kN/m
$\mu_1 = \mu_2 = 0$
$\delta_{10} = \delta_{20} = 0$

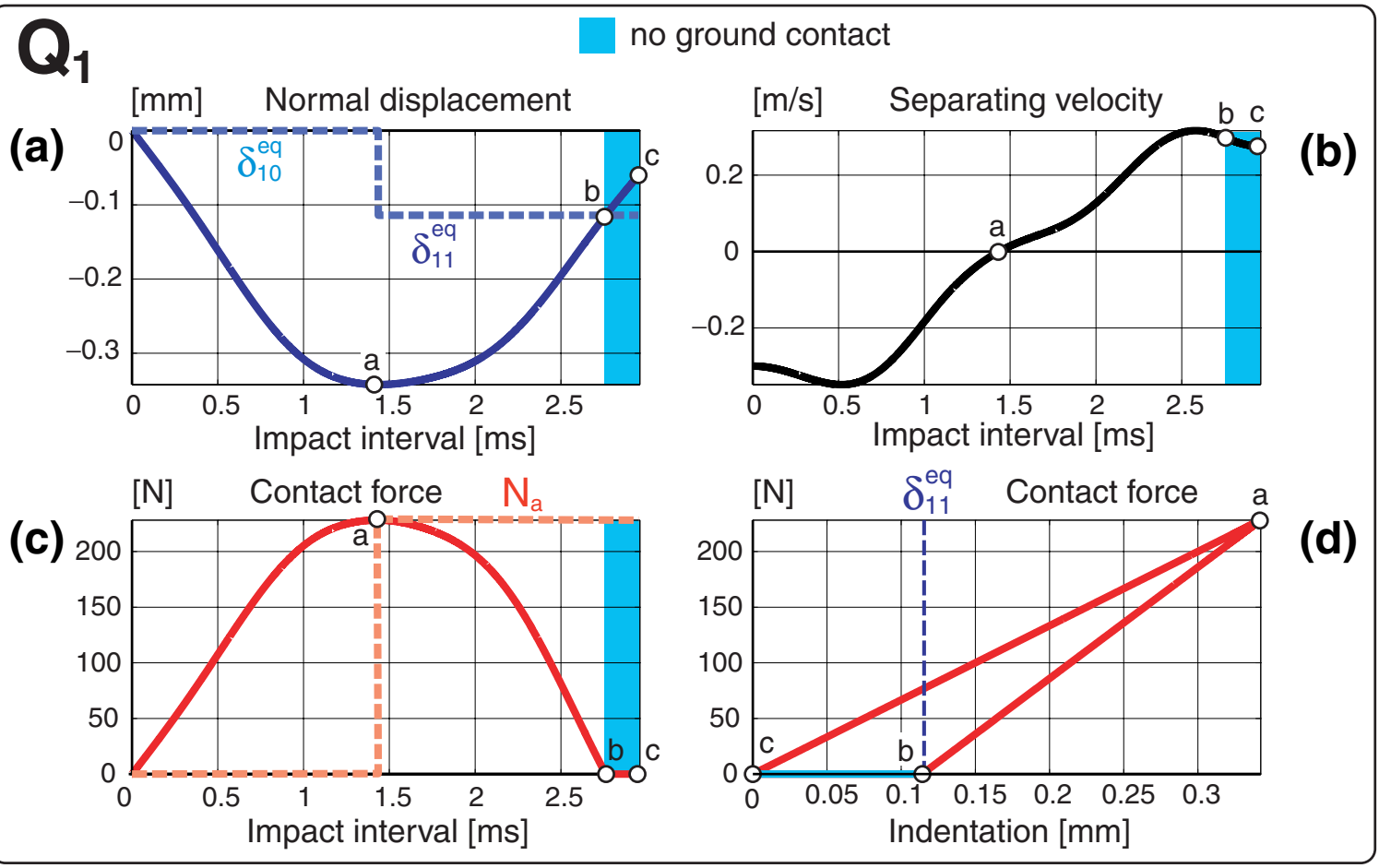

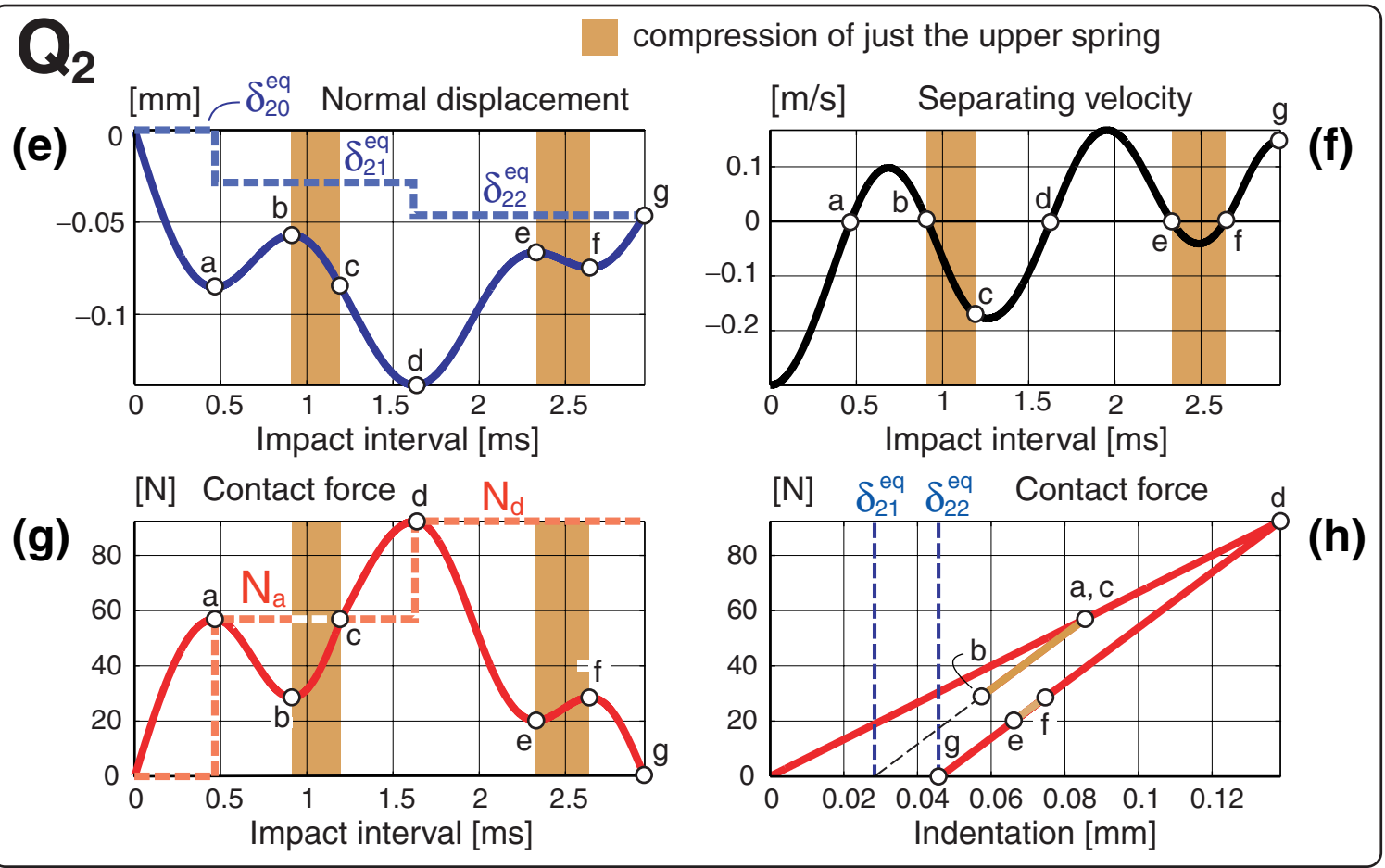

colour figure
Click here to download colour figure: Fig 11.eps

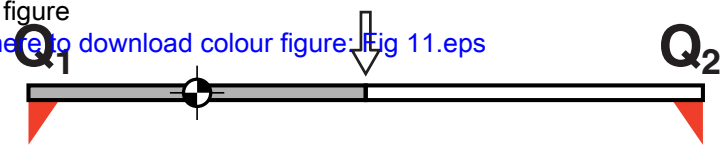

$k_1 = k_2 = k'_1 = k'_2 = 10^3$ kN/m
$\mu_1 = \mu_2 = 0.1$
$\delta_{10} = \delta_{20} = 0$

Q_1

no ground contact

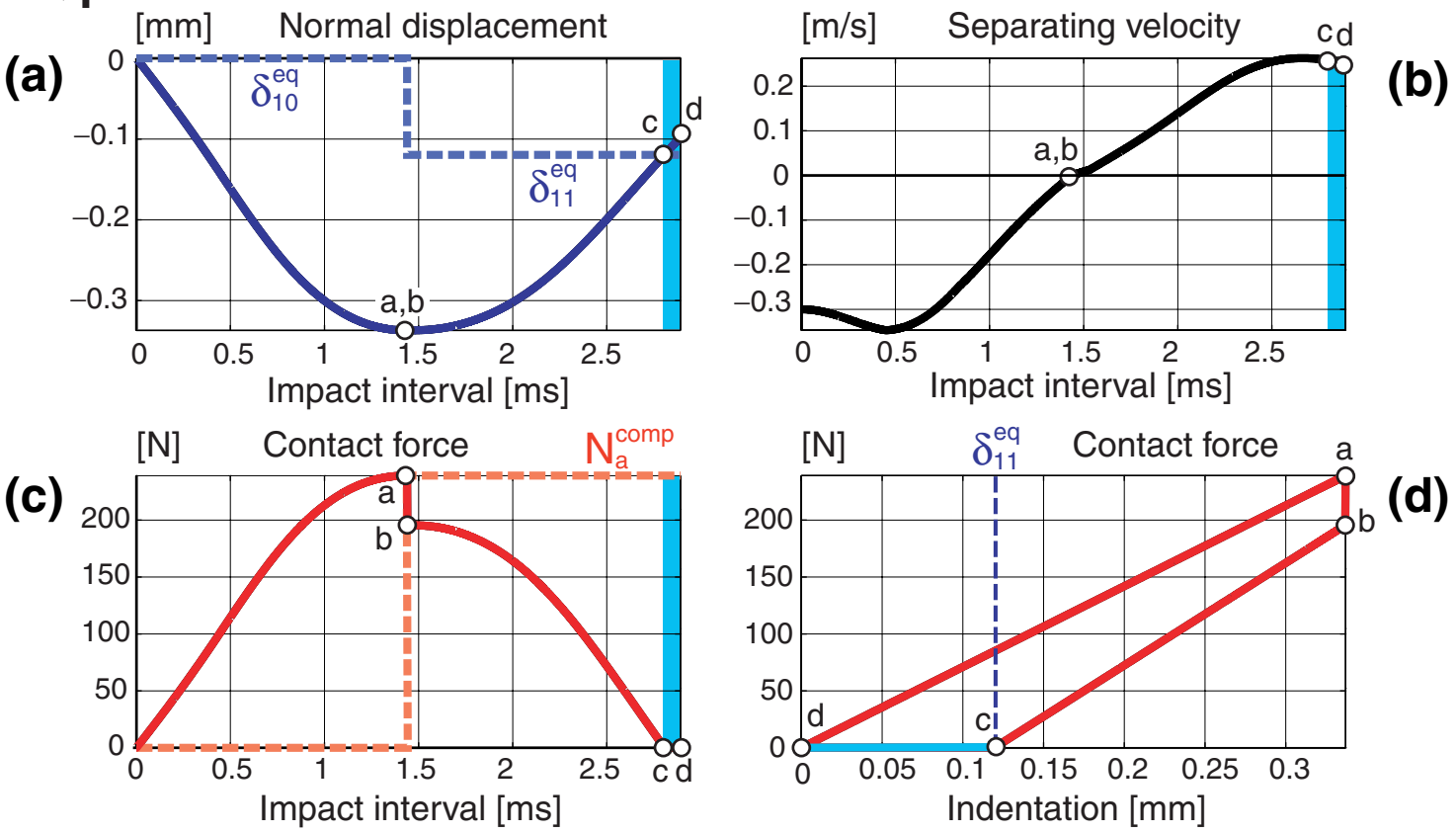

Q_2

compression of just the upper spring

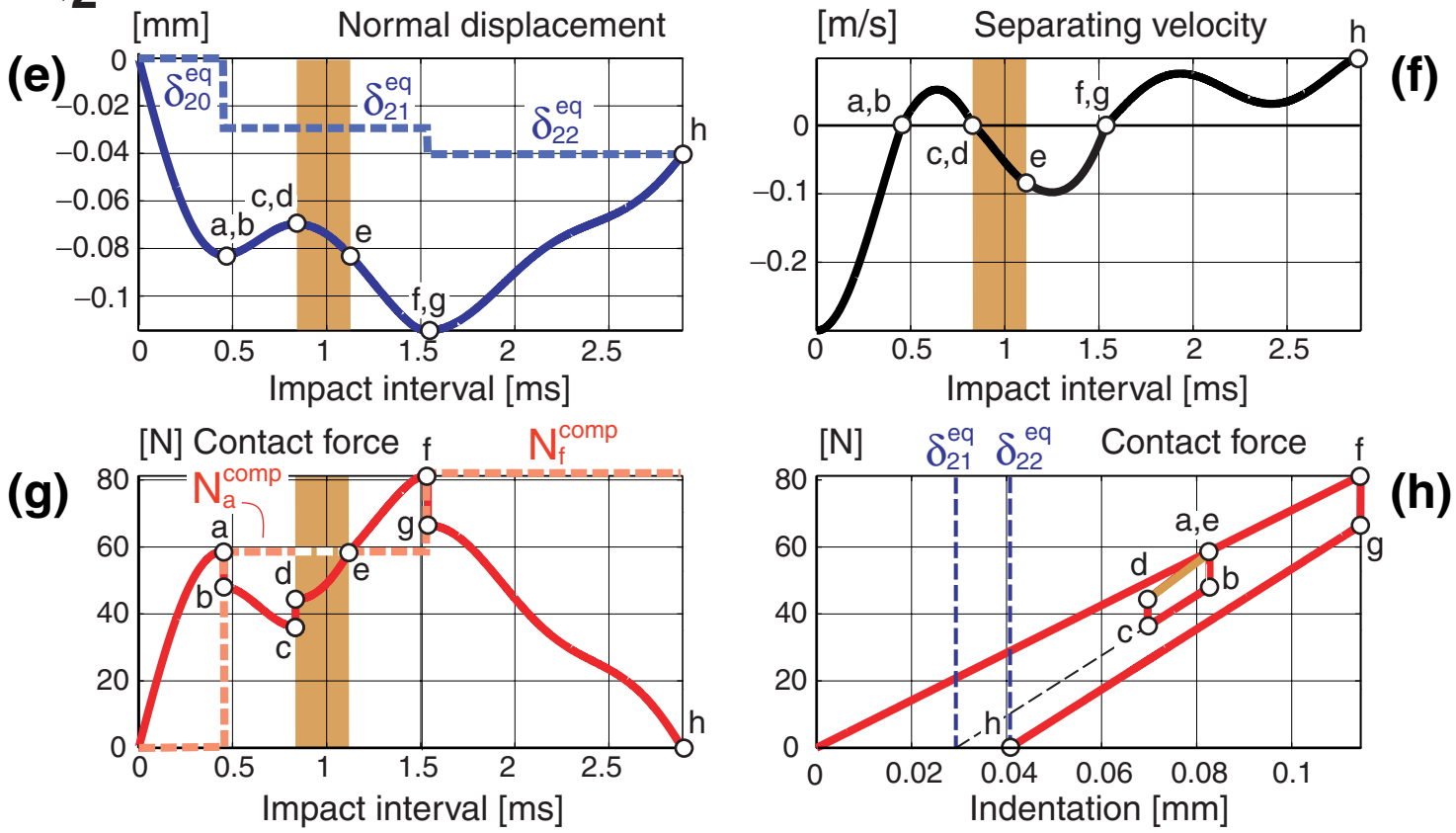

colour figure
Click here to download colour figure: Fig 12.eps

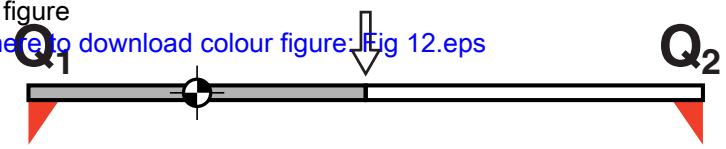

$k_1 = k_2 = k'_1 = k'_2 = 10^3$ kN/m
$\mu_1 = 0 \mu_2 = 0.3$
$\delta_{10} = 0$, $\delta_{20} = -0.1$ mm

Q_1

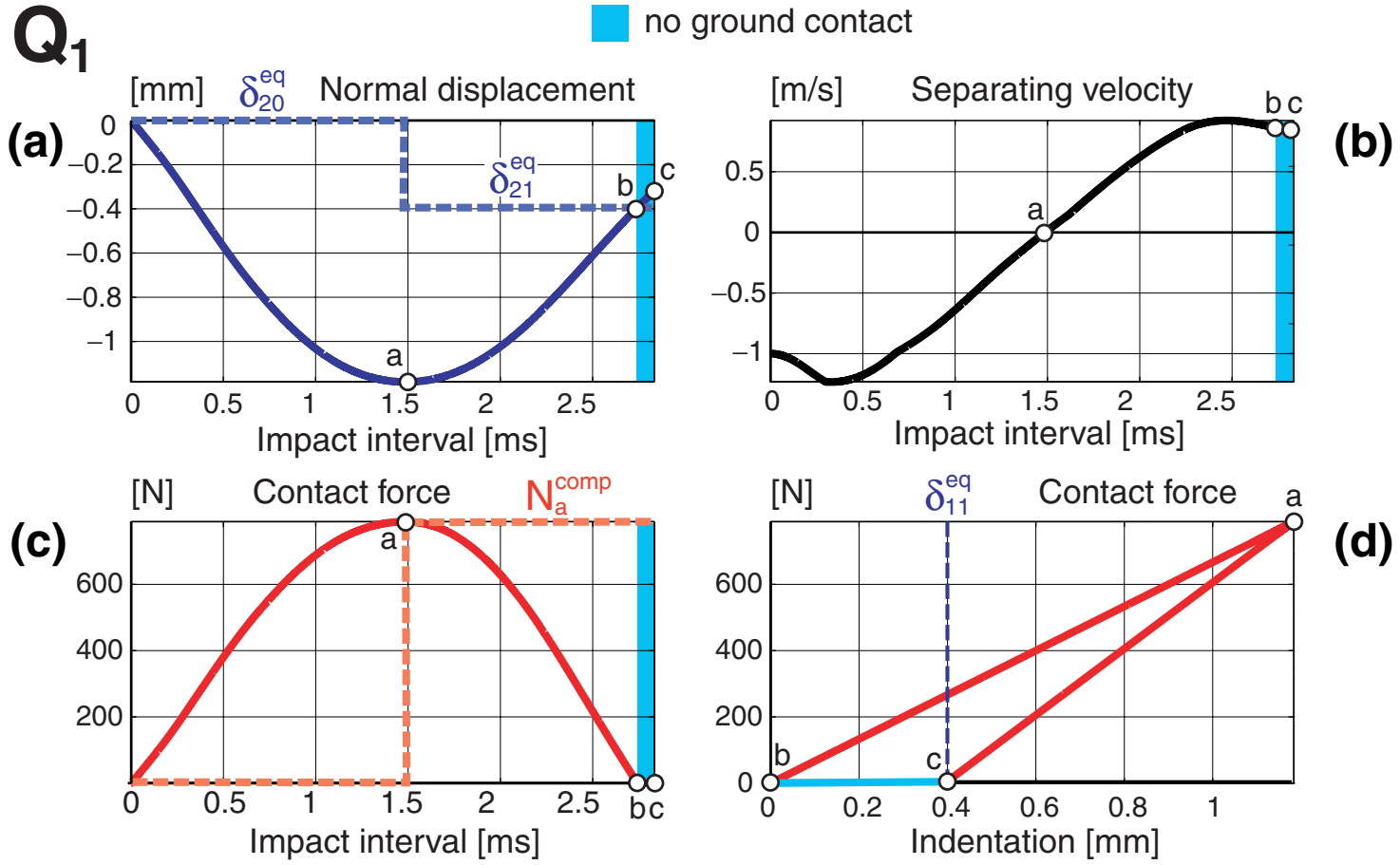

Q_2

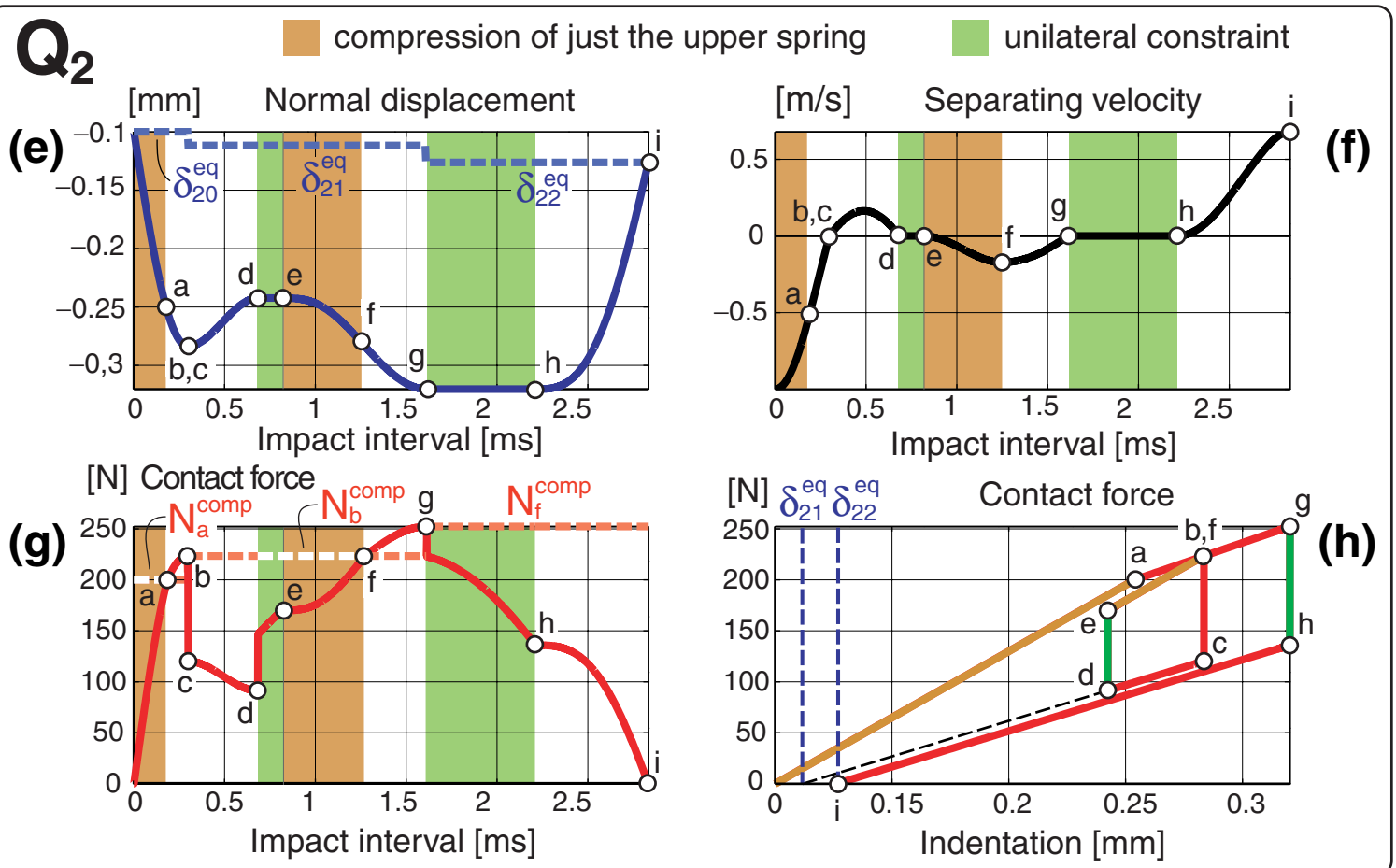

colour figure
Click here to download colour figure: Fig 13.eps

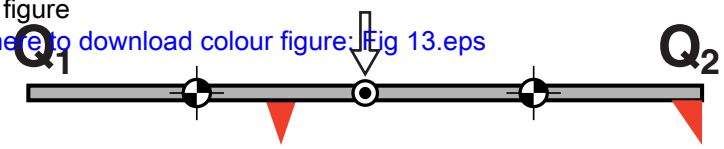

$k_1 = k_2 = k'_1 = k'_2 = 10^3$ kN/m
$\mu_1 = 0$, $\mu_2 = 0.3$
$\delta_{10} = 0$, $\delta_{20} = -0.2$ mm

Q_1

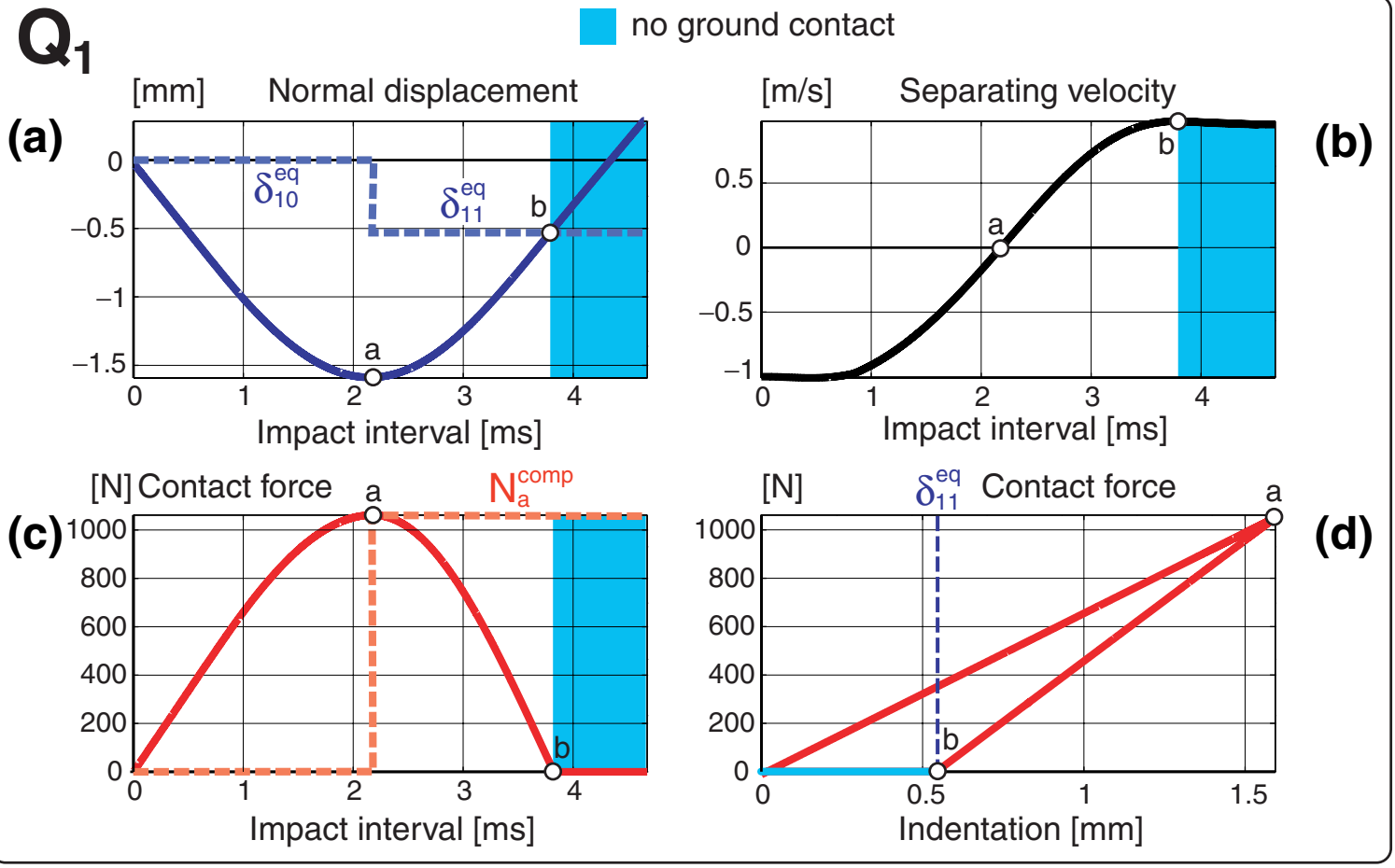

Q_2